Institut für diagnostische und interventionelle Radiologie

Klinikum rechts der Isar der Technischen Universität München

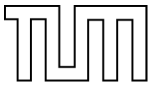

Optimization and Characterization of Magnetic Nano Particle - Vesicular Stomatitis Virus complexes for Therapy of Hepatocellular Carcinoma

Florian Wille

Vollständiger Abdruck der von der Fakultät für Medizin der Technischen Universität München zur Erlangung des akademischen Grades eines Doktors der Medizin (Dr. med.) genehmigten Dissertation.

Vorsitzender: Prof. Dr. Ernst J. Rummeny

Prüfer der Dissertation:

1. Priv.-Doz. Dr. Rickmer Braren

2. Prof. Dr. Roland M. Schmid

Die Dissertation wurde am 23.12.2015 bei der Technischen Universität München eingereicht und durch die Fakultät für Medizin am 25.06.2017 angenommen.

1 Content

2 Abbreviations

BCLC staging - Barcelona Clinic Liver Cancer staging

CPE - cytopathic effect

FCS - Fetal calf serum

GFP - Green fluorescent protein

HA - Hyaluronic acid

HBV - Hepatitis B virus

HCV - Hepatitis C virus

HCC - Hepatocellular carcinoma

LbL self-assembly - Layer by layer self-assembly

MNP - Magnetic nanoparticle

MRI - Magnetic resonance imaging

NASH - Nonalcoholic steatohepatitis

NSEM - Negative staining electron microscopy

PAGA - Poly alpha glutamic acid

PBS - Phosphate buffered saline

PEI - Polyethylenimine

Poly-GAL - Poly galacturonic acid

pfu - Plaque forming units

RFA - Radiofrequency ablation

TACE - Transarterial chemoembolization

VP - Virus particle

VSV - Vesicular stomatitis virus

VSV-PEIMag2 - Complexes of VSV and the MNP “PEIMag2”

VSV-PEIMag2-HA - Complexes of VSV and PEIMag2, shielded with HA

VSV-PEIMag2-PAGA - Complexes of VSV and PEIMag2, shielded with PAGA

VSV-PEIMag2-Poly-GAL - Complexes of VSV and PEIMag2, shielded with Poly-GAL

VSV-PEIMag2-P6YE5C - Complexes of VSV and PEIMag2, shielded with P6YE5C

3 Introduction

3.1 Hepatocellular Carcinoma: a “rising tide from east to west” (Monsour Jr, Asham et al. 2013)

Hepatocellular carcinoma (HCC) is the fifth most common cancer with over 1 million new cases annually worldwide. Due to the lack of effective therapy in comparison to other kinds of cancer, it ranks third in cancer related mortality. (Waly Raphael, Yangde et al. 2012)

When primary tumor resection is possible, 5-year survival rates are about 67%, but as early prognosis of HCC is still difficult, only few patients are eligible for this kind of therapy (Lim, Chow et al. 2012). Accordingly, the overall 5-year survival rate has remained poor at around 15% in the US (Howlader N 2012).

Several risk factors for HCC development have been identified, most of which lead to chronic liver damage with subsequent cirrhosis formation. Chronic viral infections with hepatitis B virus (HBV) and hepatitis C virus (HCV) are common in Asian countries. For example, in Japan, markers of HCV infection are found in 80 to 90% of HCC patients, whereas in Western countries this is true for only 60% of patients diagnosed with hepatocellular carcinoma with the remaining patients suffering from other conditions, such as obesity and Diabetes Mellitus type II. Those risk factors can lead to nonalcoholic steatohepatitis (NASH) and thus cause HCC formation (Gitto, Vitale et al. 2015). Considering the expected rise of obesity and Diabetes Mellitus type II, especially in the Western countries, a further increase of HCC cases in Western Europe and Northern America is to be expected (El-Serag 2011). This underlines the urgent need for new therapeutic strategies, especially in the frequent cases when a primary resection is no longer possible.

Several classification systems for HCC have been published. The general consensus, supported by the European Association for the Study of the Liver and the American Association for the Study of Liver Diseases, is that the Barcelona Clinic Liver Cancer (BCLC) staging should be preferred (see figure 1).

According to the BCLC staging system HCC patients are classified in five categories: very early, early, intermediate, advanced, and terminal.

For patients who are diagnosed in a very early stage (BCLC stage 0), surgical resection is the therapy of choice; however, this modality is reserved for patients with tumors that are singular, smaller than 2cm in diameter and have no portal hypertension or elevated bilirubin levels. This is true for only approximately 5% of patients diagnosed with HCC in Western countries (El-Serag, Marrero et al. 2008). When diagnosed early, but not meeting the criteria for resection, the next step in the current HCC therapy scheme is organ transplantation. Here, recurrence rate is low and 5-year survival rates are over 70%. But this is only possible due to strict selection criteria (Milan criteria: singular lesion smaller than 5 cm or up to 3 lesions smaller than 3 cm and no extrahepatic manifestations and no vascular invasion (Mazzaferro, Regalia et al. 1996)), which makes liver transplantation a successful therapy, but not applicable to the large number of patients who would require it.

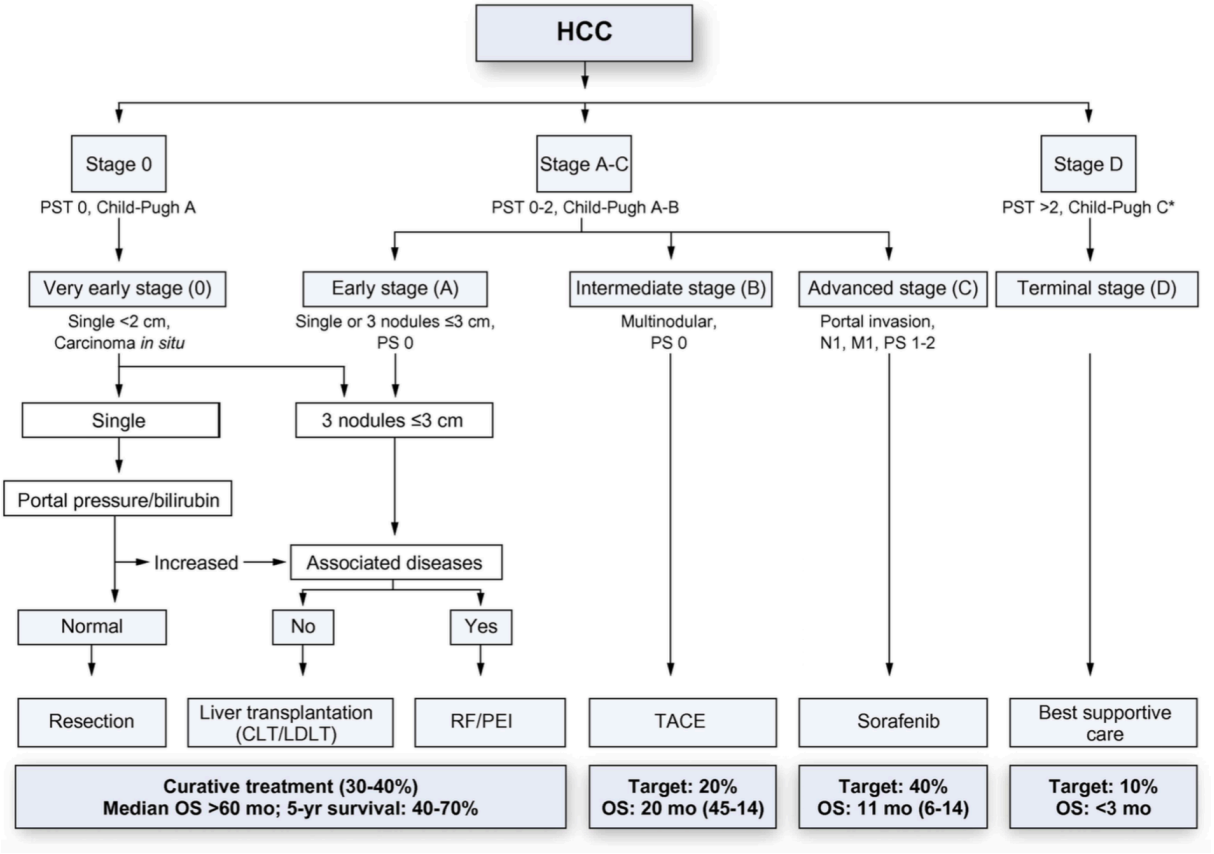

Figure 1: Updated BCLC Staging system and Treatment Strategy (European Association For The Study Of The, European Organisation For et al. 2012)

Radiofrequency ablation (RFA) is another potentially curative option. It is still only applied when primary resection is not applicable, though a randomized clinical trial showed no disadvantage in survival rates after RFA in comparison to primary resection. (Chen, Li et al. 2006)

A very frequently used method to either treat patients in an intermediate state of tumor progression, or to bridge time between diagnosis and a possible liver transplantation, is transarterial chemoembolization (TACE). It is considered to be a palliative treatment, and thus, is only used with larger tumors that cannot be resected or with multifocal lesions.

When diagnosed at an advanced tumor stage with portal invasion and/or metastases, the treatment of choice is Sorafenib. This oral multikinase inhibitor has been shown to improve symptom free and overall survival for those patients (Llovet, Ricci et al. 2008).

As can be seen, there remains a shortage of clinically available treatment options to help patients in the continually growing number of cases of hepatocellular carcinoma, which is why novel therapeutic strategies for this disease are being sought worldwide.

3.2 Oncolytic Virotherapy with Vesicular Stomatitis Virus

One of these novel treatments is the use of oncolytic viruses. Antitumor success for several different cancer modalities has been made with different types of virus, and promising results have been achieved with (partially genetically modified) Adenovirus, Newcastle Disease Virus, Vaccinia Virus, Measles Virus and Vesicular Stomatitis Virus, all of which are currently being tested in clinical trials. (Russell, Peng et al. 2012)

For this project, we chose to use Vesicular Stomatits Virus (VSV), a bullet shaped negative strand RNA virus from the family of Rhabdoviridae. It naturally infects cattle, horse and swine and leads to a relatively harmless infection, but with symptoms mimicking those of early foot-and-mouth-disease virus, which is feared by farmers and veterinarians. For humans, VSV is generally non-pathogenic, although mild flu-like symptoms have been reported. Because of its low virulence to humans, the prevalence of antibodies

Figure 2: Negative staining electron microscopy of VSV-GFP

against VSV is generally extremely low, except for some areas in Georgia, USA and Central America, where VSV is endemic. (Lichty, Power et al. 2004)

As it has a short replication cycle and has shown promising oncolytic properties in several in vitro and animal studies, VSV is the perfect candidate for our in vitro and in vivo experiments (Balachandran and Barber 2000, Lichty, Power et al. 2004, Naik, Nace et al. 2012). There is a clinical trial for HCC currently being conducted at the Mayo Clinic, USA, where a genetically modified VSV expressing IFN-beta is used (Russell, Peng et al. 2012). It is hypothesized that, through this modification, the therapeutic index will be improved, and possible neurotoxic side effects that have been observed in Macaques (Johnson, Nasar et al. 2007) are expected to be avoided. Apart from neurotoxicity, effective systemic application of VSV for tumor therapy faces major challenges such as premature clearance from the body, low virus levels in the target area and strong immunogenicity leading to production of neutralizing antibodies (Hastie and Grdzelishvili 2012).

3.3 Magnetic targeting with magnetic nanoparticles

The use of magnetic nanoparticles (MNPs) in complexes with Vesicular Stomatitis Virus (VSV) has the potential to improve oncolytic virotherapy on several levels. First, in magnetically active complexes, VSV could be enriched to the tumor area by the application of an external magnetic field. This would potentially lead to higher specific effects while decreasing systemic side effects. Secondly, when surrounded by MNPs, the virus is protected from the host immune system to a certain extent, which could help improve virus circulation time and reduce induction of a specific immune response. Finally, virus delivery can be monitored using MRI imaging, as MNPs

change the local relaxivity and lead to an MR signal loss (Chertok, Moffat et al. 2008, Mykhaylyk, Sobisch et al. 2012).

The feasibility of this approach was shown, for example, by Tresilwised et al, who applied complexes of oncolytic virus and MNPs as a therapy for tumor xenografts in mice using magnetic targeting strategies (Tresilwised, Pithayanukul et al. 2010).

3.4 Aim of this study

The overall aim of this study was to optimize VSV-MNP complexes for therapeutic application in HCC. Specifically, we wanted to:

1. Identify optimal ratios of PEI-Mag2 and VSV for VSV-MNP self-assembly
2. Characterize different shielding polymer surface coatings on VSV-PEIMag2 complexes.

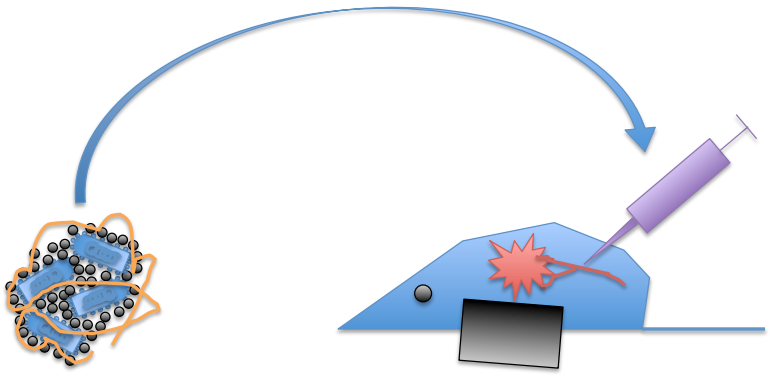

3.5 Physical/biochemical background

This thesis is based on experiments using magnetic iron-oxide nanoparticles complexed with Vesicular Stomatitis Virus and eventually shielded with negatively charged biopolymers. For better understanding, the following section will provide a short explanation and summary of the important physical/biochemical principles involved:

3.5.1 Layer by layer self assembling technique

The technique of layer by layer self assembling has been used for decades to construct multicomposite molecular assemblies of tailored structure (Decher 1997). It is based on a simple principle: a charged substrate is covered with molecules bearing the opposite charge. They are attracted and fixed to the surface by electrostatic interactions. This step is then repeated, as the resulting surface can now be covered by different macromolecules bearing the opposite charge, and so on and so forth. This leads to a well-organized multilayered structure. (See figure 3)

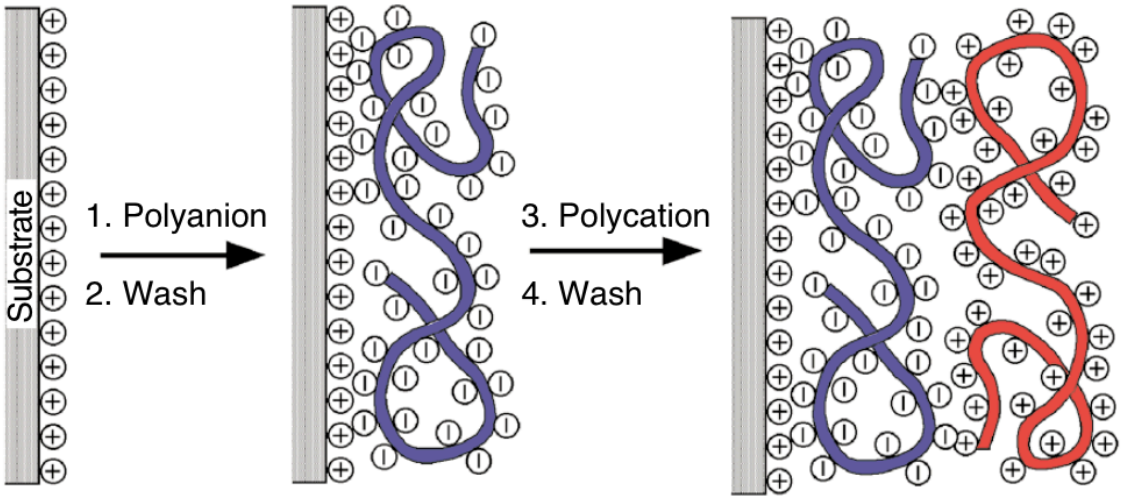

Figure 3, from: Decher, G., Fuzzy Nanoassemblies: Toward Layered Polymeric Multicomposites. Science, 1997. ***277****(5330): p. 1232-1237*

In the first years, emphasis laid on improvement of plane self-assembled structures and their characterization. Already in this phase, viral particles were also used in place of a polyanions to become a part in the desired multilayered structure (Lvov, Haas et al. 1994). Recently, however, virus particles have even been used as the actual substrate for layer by layer (LbL) self-assembling, resulting in three dimensional structures surrounded by layers of polyanions and cations (Plank, Zelphati et al. 2011). When those virus particles (e.g. adenovirus) are covered with cationic magnetic nanoparticles, this leads to viral particles that are still infective, but at the same time, susceptible to magnetic force. Plank et al. described in their recent review a method of creating virus-MNP complexes that can be seen as a modification of the classical LbL self assembly technique: in contrast to the previously described method, here, only 1 or 2 layers of oppositely charged structures are used to form complexes with uncoated or coated viruses, but still forming layers utilizing the electrostatic interactions between oppositely charged molecules (Plank, Zelphati et al. 2011). (See figure 4)

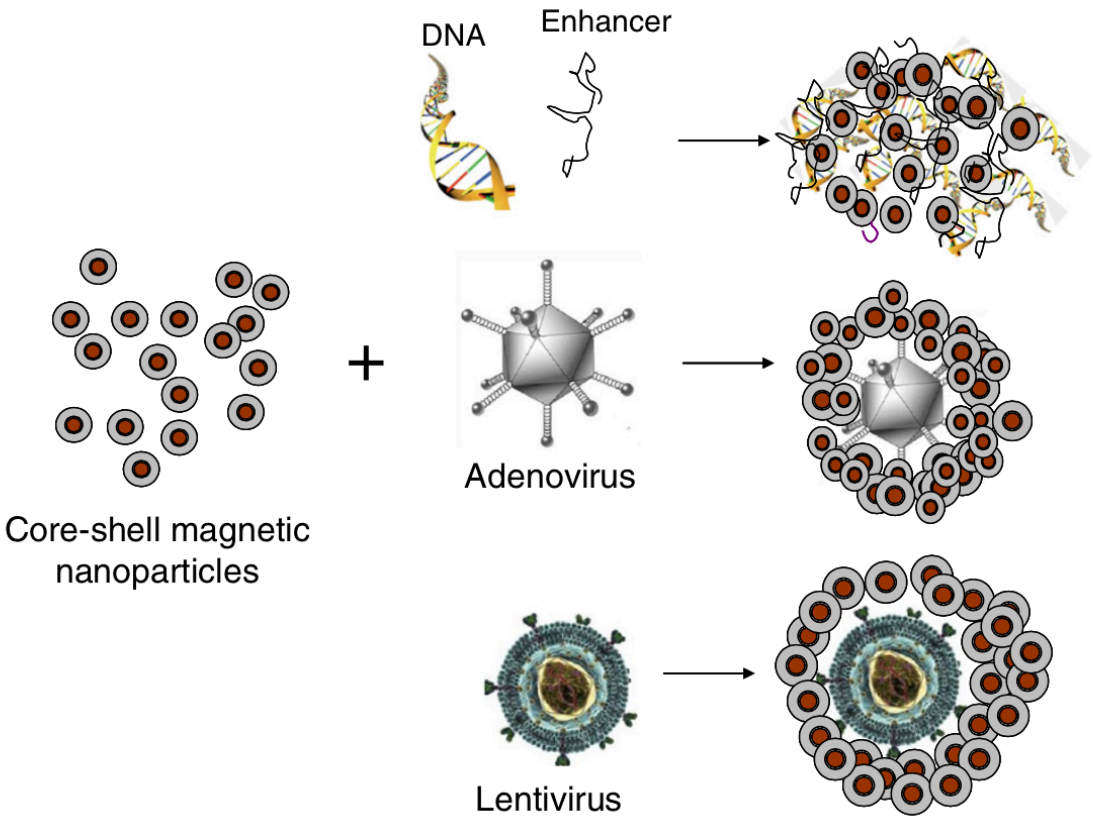

Figure 4, from: Plank, C., O. Zelphati, and O. Mykhaylyk, Magnetically enhanced nucleic acid delivery. Ten years of magnetofection-progress and prospects. *Adv Drug Deliv Rev, 2011.* ***63****(14-15): p. 1300-31.*

3.5.2 Stability of a colloidal system

As it is widely known, surface charge plays a crucial role in a colloidal solution (a system in which small particles of 1nm to 10um are evenly distributed in a liquid (Britannica 2015)) and has a strong impact on its stability. The neutral charge of these distributed particles is associated with fast clotting and solution instability, whereas a stronger surface charge - positive or negative - results in improved colloidal stability, due to repelling electrostatic interactions between the equally charged particles. This is true for “simple” colloids and plays an important role in

many different industry branches, e.g. in the pharmaceutical and cosmetics fields, where colloidal solutions are designed to be stable for a certain amount of time. However, when a colloidal solution is administered in vivo, conditions are far more diverse: even if human blood can be seen as a complex active colloidal system, the exact mechanisms of interactions between the many different blood components – cellular as well as plasmatic – is still not totally clear (Voeikov, Buravleva et al. 2011). Of course some things are known: red blood cells, for instance, are prevented from clotting due to their negative surface charge (Jan and Chien 1973). In addition, plasma proteins (mainly serum Albumin) bear a net negative charge at physiological pH.

For nanoparticles administered in vivo, it has been shown that an important factor for fast elimination from the blood flow is plasma protein interactions. This effect becomes stronger in direct correlation to the degree of positive charge of the administered nanoparticle, which can be understood considering the negative charge of albumin and other plasma proteins (Soheyla H 2013). Furthermore, positively charged nanoparticles appear to have stronger cytotoxic effects on healthy cells, which can be reduced by making their charge negative through shielding (Unger, Wittmar et al. 2007). On the other hand, positively charged nanoparticles also showed advantages in their performance, for example, regarding targeted drug delivery, which outlines the complexity of this topic (Soheyla H 2013). It can be summarized that the surface charge of particles that are to be injected in vivo has an effect on the stability of the particles and their interactions with blood components, and that the exact optimum charge depends on the intended use of the therapeutic agent.

3.5.3 Magnetic nanoparticles in medicine

The concept of injecting magnetically active particles in the body is not a new one: it has been over 25 years since the use of magnetic micro- and nanoparticles as carriers for drug delivery was proposed, and already in the 1960's, magnetic fluid compounds were injected to occlude cerebral and renal aneurysms (Alexiou, Jurgons et al. 2003, Kim, Shin et al. 2012). Since then, many different possible applications for the use of magnetic nanoparticles have been suggested: as hyperthermia agents under application of a high frequency magnetic field, as magnetic carriers that are directed in a desired area in the body by an external magnetic field, as a means for tissue engineering, and last but not least, as contrast agents in magnetic resonance imaging (MRI) and in magnetic particle imaging (MPI) (Polyak and Friedman 2009). The most commonly used particles in this field are superparamagnetic iron oxide particles. The reason for the use of these nanoparticles (showing superparamagnetic properties) lies in the combination of two different requirements: first of all, the particles should have a strong magnetic moment, because only through this an external magnetic field can apply an actual force over a certain distance. Secondly, the magnetization should stop without the external magnetic field, because otherwise the particles would interact magnetically with each other and form aggregates. For this reason, ferromagnetic and ferrimagnetic materials are not used for in vivo application. Additionally, as paramagnetic materials only magnetize weakly in an external magnetic field, superparamagnetic nanoparticles are the first choice, as they combine the advantageous properties of the other types of magnetic materials (Polyak and Friedman 2009).

4 Materials and Methods

4.1 Cell culture

Morris Hepatoma Cells, McA-RH7777, were cultivated at 37°C in a humidified atmosphere containing 5% CO2. As culture medium, Dulbecco's modified Eagle's medium (DMEM) with 10% fetal calf serum (FCS) and 1% Penicillin/Streptomycin was used.

The BHK-21 cells used for virus replication, plaque assays and infectivity assays were cultivated under the same conditions, but with Glasgow Minimum Essential Medium (GMEM) with 10% fetal calf serum, 1% Penicillin/Streptomycin and 1% Tryptose phosphate as cell culture medium.

4.2 Vesicular Stomatitis Virus expressing GFP (rVSV-GFP)

The rVSV-GFP stock was grown and amplified in 90% confluent BHK-21 cells in OptiPRO medium. After infection at a multiplicity of infection of 0,0001 and incubation for 48 hours, the supernatant was collected and purified by ultracentrifugation in a sucrose gradient as described by Altomonte et al (Altomonte, Braren et al. 2008). The resulting stock had a titer of 1,66E10 pfu/ml (measured by a standard 6-well-plate plaque assay in triplicate) and was stored in aliquots of 100ul at -80°C.

4.3 Magnetic Nanoparticles

The magnetic nanoparticles used in this project were a kind gift from Olga Mykhaylyk/AG Plank. They are core shell type iron oxide MNPs synthesized by precipitation of Fe(II)/Fe(III) hydroxide from an aqueous solution of Fe(II)/Fe(III)-salts

followed by tranformation into magnetite in an oxygen-free atmosphere. Afterwards, a surface coating consisting of the fluorinated surfactant ZONYL FSA (lithium 3-[2-(perfluoroalkyl)ethylthio] propionate) combined with 25-kDa branched poly(ethylene imine) (PEI-25Br) was added. The resulting magnetic nanoparticles are referred to as PEI-Mag2. (Mykhaylyk, Antequera et al. 2007, Plank, Zelphati et al. 2011)

4.4 Complex formation and Fe/pfu ratio titration

Complexes of VSV and PEI-Mag2 were formed in PBS by electrostatic interactions between the positively charged MNPs and the negatively charged VSV in analogy to the protocol of Tresilwised et al (Tresilwised, Pithayanukul et al. 2012). Assembly was performed at a final virus concentration of 1E8 pfu/ml. To find out the optimum ratio of PEI-Mag2 to VSV, complexes were created with a dilution series of PEI-Mag2 in ddH2O, leading to final Fe/pfu ratios from 5 to 5000 fgFe/pfu. To this MNP:water dilution, the virus in PBS dilution was added in order to receive the right final virus concentration and Fe/pfu-ratio. The solution was then gently agitated by pipetting up and down and incubated under the cell culture hood for 20 minutes to allow complexes to form.

An exemplary titration scheme for creation of 1ml of complex solution with a ratio of 300 fgFe/pfu is shown in Table 1.

Virus stock	1,66E+10	pfu/ml
PEI-Mag2 stock	2,5E+12	fgFe/ml
Assembling at	1,00E+08	pfu/ml
For 1 ml of complexes at 300fgFe/pfu:		
Virus diluted in	0,8	ml
PEI-Mag2 diluted in	0,2	ml
Virus dilution:		
Virus stock	6,02	µl
PBS	793,98	µl
MNP dilution:		
PEI-Mag2 stock	12,00	µl
Water	188,00	µl

Table 1: Exemplary titration scheme for VSV-PEIMag2 complexes at 300fg/pfu

4.5 Size and charge measurements

For measurement of the size and charge of the virus particles, complexes and shielded complexes, a Zetasizer Nano ZS (Malvern, Herrenberg, Germany) was used. This instrument estimates the size of particles using the Dynamic Light Scattering technique. The zeta potential is measured following the principle of Laser Doppler Velocimetry (Malvern_Instruments 2004).

4.6 Magnetic responsiveness

To examine the magnetically induced velocity (magnetic responsiveness) of the magnetic complexes, the time course of the turbidity of the suspensions when subjected to inhomogeneous magnetic fields was measured, as described previously by Mykhaylyk et al (Mykhaylyk, Zelphati et al. 2008). Briefly, a gradient field was generated by positioning two mutually attracting packs of four quadrangular neodymium-iron-boron permanent magnets symmetrically on each side of a cuvette holder parallel to the light beam of the spectrophotometer (DU-640, Beckman). The magnetic field between the magnets was measured using a grid of step size 1 mm, and the average magnetic field and resulting field gradient perpendicular to the measuring beam were calculated to be 213 mT and 4 ± 2 T/m, respectively. Aliquots of the suspensions of the complexes were diluted to achieve a starting optical density of 0.4– 1 at the analytic wavelength. An optical cuvette filled with one of these diluted suspensions was then placed into the holder of the spectrophotometer and exposed to a magnetic field, and the optical density (turbidity) was recorded at 360 nm in kinetic mode. The resulting clearance curves were drawn by plotting the normalized optical densities at the analytical wavelength (OD_{360}/OD_{360}) against time. From these curves, the time to magnetic sedimentation of 90% of magnetic complexes $t_{0.1}$ [s] was deduced, and the average magnetophoretic mobility of the free complexes and labeled cells was calculated as $v_z = 10^3/t_{0.1}$ [µm/s] (accounting for the average path of 1 mm in the experimental setup). In a stationary regime, the hydrodynamic force counterbalances the magnetic force that acts on a particle assembly, such as a magnetic vector comprising multiple magnetic nanoparticles, and the derived magnetophoretic mobility of the complexes and the average hydrodynamic diameter of the objects D_h allows one to estimate the average magnetic moment M and finally

the average number of magnetic nanoparticles associated with the complex $N=M/m_{eff}$ (accounting for the effective magnetic moment of the insulated MNP in the applied field). This approach was used by Wilhelm et al. when analyzing the magnetophoretic mobility distribution from cell tracking experiments. This description was written according to the publication of Grzeskowiak et al (Grzeskowiak, Sanchez-Antequera et al. 2015).

4.7 Magnetic sedimentation and quantification of virus titer in supernatant

In order to specify the Fe/pfu-ratio at which most of the virus is bound to the complexes, the principle of magnetic sedimentation was used. The idea was to measure the amount of virus that is bound in the complexes at different Fe/pfu-ratios and thus can be attracted by magnetic force. For this purpose, a permanent magnet stack was used in which 1ml Eppendorf cups can be mounted so that the magnetic force draws the complexes to one bottom side of the cup. (See figure 5)
After complex formation as described above, samples of 300µl containing different Fe/pfu ratios were magnetically sedimented for 20 minutes, and 100µl of the supernatant were carefully removed and examined for virus titer in a TCID50 assay. For all TCID50-assays, the resulting titer was calculated using the TCID50 calculator by Binder, M., Universitätsklinikum Heidelberg (Binder 2013).

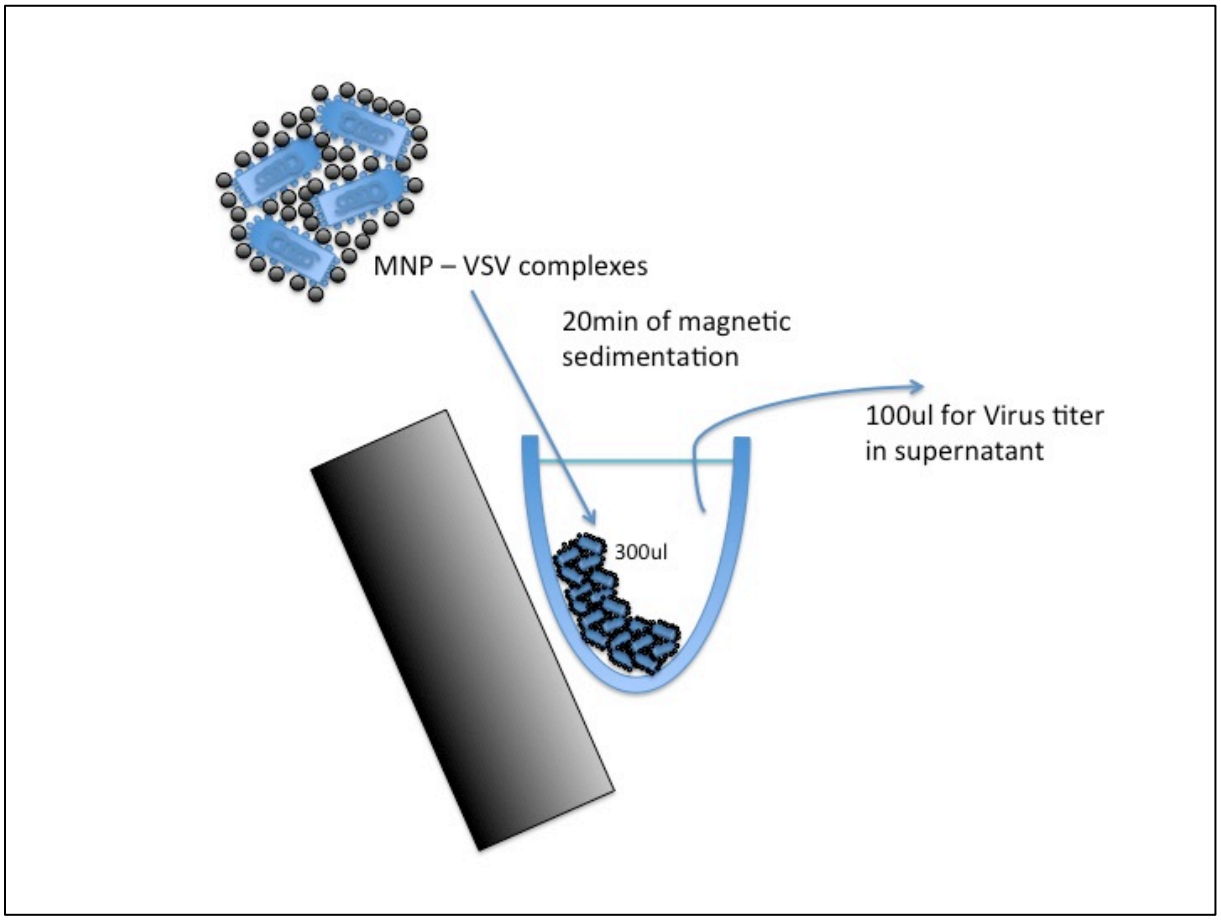

Figure 5: experimental set-up for the magnetic sedimentation assay

4.8 Negative Staining Electron Microscopy

In order to visualize the complexes, negative staining electron microscopy (NSEM) was used. Complexes were formed as described above and then loaded on negative staining electron microscopy grids that were purchased from Plano GmbH, Wetzlar. Standard NSEM protocols for virus staining use a drop of the virus containing sample with a grid placed on top of it (Hajibagheri 1999). The resolved virus thus becomes attached to the grid by hydrophilic interactions. For this special application, the protocol for visualizing the samples containing complexes of VSV and PEI-Mag2 was changed, as they are relatively big and sediment quickly. For that reason, the grid was placed on a parafilm-covered magnet, the sample then applied on top of it and allowed to sediment magnetically for 10 minutes. The fluid was then removed by

carefully touching the drop with the edge of a filter paper. Now the grid was laid on top of a drop of Uranylacetate for 1min for negative contrasting, and finally, the remaining fluid was again removed with the edge of a filter paper and the grid was air-dried. Photographs were then taken at the electron microscope of the Veterinary Pathology Department, LMU, München.

4.9 Shielding Polymers

For shielding against possible serum protein interactions and inactivation, the effect of 4 different negatively charged shielding-polymers was examined:

- Poly-alpha-glutamic acid (PAGA): a synthetic biopolymer that has advanced as a promising platform for drug delivery and is, for instance, being tested clinically as a conjugate with paclitaxel in a phase III clinical trial (Melancon and Li 2011).
- Hyaluronic acid (HA): a biopolymer that can be found in the whole human body, especially in connective tissues as in the skin, vitreous body or in the synovial fluid (Fraser, Laurent et al. 1997). There has been over 30 years of clinical experience in the use of HA for medical products, e.g. for patients suffering from Osteoarthritis (Burdick and Prestwich 2011). Recently, HA (and its receptor - CD44) has been shown to be related to tumor malignancy in some kinds of cancer and, finally, to be beneficial in improving the transduction efficiency of therapeutic and diagnostic agents, all of which makes HA a good candidate to test for shielding of the VSV-MNP complexes (Josefsson, Adamo et al. 2011, Choi, Saravanakumar et al. 2012).

- Poly-Galacturonic acid (Poly-GAL): a polysaccharide playing an important role in the plant cell wall that is used in food gels, cosmetics, and also as a drug delivery agent.
- P6YE5C: another negatively charged biopolymer with an average molecular weight of 6000 Da that was developed for enhancing the transduction efficiency of non-viral gene vectors by Finsinger et al (Finsinger, Remy et al. 2000), but has also been efficiently used by Anton et al. for magnetic transduction of adenoviral vectors (Anton, Wolf et al. 2012).

The shielding procedure was always performed as follows: complexes were created as described above at an iron/pfu-ratio of 300fgFe/pfu. After 20 minutes of incubation, these complexes were added to a PBS-dilution of the respective polymer, containing an amount of polymer that was calculated to achieve a final polymer-to-iron-ratio (w/w) between 0,01 and 10, depending on the shielding effect aimed for. For this study, 375µl of Polymer/PBS dilution was used, followed by addition of 125µl of VSV-MNP complexes (if more resulting shielded complexes were needed, a multiple of the described aliquots was used, but always keeping the same relations between the different dilutions). This mixture was then gently pipetted up and down and allowed to incubate for another 15 minutes. Now the shielded complexes were ready to be used for further experiments.

4.10 Infectivity measured by GFP expression after shielding

For examining the effect of shielding of the VSV-MNP complexes on infectivity, GFP expression 10h after infection was measured. For this purpose, complexes were created as described above, followed by shielding with one of the 4 polymers of interest. Each polymer was tested in 9 different polymer to iron (w/w) ratios, ranging

from very low amounts of polymer until high concentrations (0,01 to 10 times the iron concentration).

The resulting agents were carefully pipetted into 24-well plates containing 80% confluent Morris cells, 24h after splitting. This was followed by 20 minutes of incubation at 37°C, either with or without application of a magnetic field.

The complete media was then removed and replaced by dye-less culture media without FCS, and the plates were incubated for 10 hours. Pictures of representing wells were taken under bright field and fluorescent light, and finally the cells were lysed by simply adding a twice-concentrated TritonX-Cell-Lysis buffer.

Measurement of the GFP signal was then carried out using a plate reader by pipetting the 200µl lysates into a black-walled 96 well plate.

Note: It was necessary to infect in 24-well rather than in 96-well plates (which would have been more practical, as measurements in the plate reader are performed in the latter) because, only with a higher cell number, the signal-to-noise ratio was high enough to obtain informative results.

4.11 Neutralizing antibody assay

VSV, VSV-PEIMag2 and VSV-PEIMag2-HA (at low and high dose of hyaluronic acid shielding with a polymer to iron w/w ratio of 0,1 and 10) were incubated in rat VSV-antiserum (produced by immunization of buffalo rats with the VSV-GFP stock by giving two injections at day 0 and day 7 and collection of serum at day 14) for 120 minutes. This was followed by an assay similar to the TCID50 assay to examine the highest serum titer at which there was no CPE to be observed after 48 hours.

In detail, complexes were formed with an iron/pfu-ratio of 300fgFe/pfu. Shielding was then performed by adding the complexes to a PBS-dilution of hyaluronic acid as

described above. The resulting shielded complexes and negative controls were now diluted to a concentration of 500pfu/ml, and 100µl aliquots were each pipetted onto a dilution series of the antiserum (quadruplicates on a 96 well-plate). These 96-well plates were now incubated at 37°C for 120 minutes. After this, the incubated samples were transferred to 96-well plates confluent with BHK-21 cells analog to the above-mentioned TCID50 assay. After 48h, the cytopathic effect (CPE) was evaluated, and thus, the antiserum concentration needed to inactivate all of the VSV in the respective sample could be calculated. The experiment was repeated for a total of 5 times (n=5).

4.12 In vivo half life of shielded complexes

All procedures involving animals were approved and performed according to the guidelines of the institutions animal care and use committee and government of Bavaria, Germany.

In order to assess the kinetics of VSV, VSV-MNP complexes and shielded complexes in vivo, 4-6 week old Buffalo rats were anesthetized by isoflurane anesthesia. Once the rats were asleep, they were weighed, shaved at the ventral neck area, and a tail vein catheter was established. Now, a small incision was made from the ventral shoulder towards the clavicle, according to the protocol of Thrivikraman et al (Thrivikraman, Huot et al. 2002). By careful preparation, the jugular vein was exposed and prepared in a caudal direction to the point where it is joined by the subclavian vein. Once there was a clear view of this confluence, a 22G catheter was inserted into the angle of the veins and carefully pushed forward until the whole tip of the catheter was inside the vein (See figure 6). After assuring the correct position of the catheter by checking for blood backflow, a first blood sample of

350µl was obtained as a baseline value. This was then divided into one part of 100µl for whole blood analysis that was immediately put on liquid nitrogen, and another part of 250µl that was first centrifuged at 2000xg for 10 minutes in order to receive a plasma sample, and then also frozen in liquid nitrogen. At this point, VSV, VSV-MNP-complexes or shielded complexes, at a dose of 2,5E7 pfu, were administered through the tail vein catheter. At certain time points (1', 2', 3', 5', 10') blood sampling was repeated as described above. Finally, all samples were stored at -80^{o}C for VSV titer analysis by TCID50 assay.

Figure 6: Experimental set up for repeated blood-taking and analysis of viral titer kinetics.

4.13 Rat HCC model

4.13.1 Implantation of Morris Hepatoma Cells 7777

For the orthotopic rat hepatoma model, McA-RH7777 cells were transplanted into the liver as described by Ebert et al (Ebert, Shinozaki et al. 2003). Briefly, 4-5 week old Buffalo rats were anesthetized with 3% Isofluran at 1l oxygen per minute. After analgesic medication with Temgesic, Rimadyl and Metamizol, the abdominal wall was opened and the anterior liver lobe was gently exposed and put down on a moist compress. Then, $4x10^6$ Morris hepatoma cells (72h after splitting, 80% confluent) were injected subcapsularly in a volume of 20µl serum free DMEM. The site where the needle had been inserted was cauterized immediately after extraction in order to avoid tumor cell spreading in the peritoneal cavity. After relocation of the liver into the abdomen, a continuous suture was placed to close the abdomen, and finally, a skin suture was set. The rats were released into veterinary care until the tumors had the desired size for further experiments.

4.13.2 Intra-arterial injection of the therapeutic agent

After approximately 10 days, the tumors were of appropriate size to proceed with the second step of the experiment: the intra-arterial injection of VSV, VSV-PEIMag2 complexes or shielded VSV-PEIMag2 complexes into the rodents' hepatic artery. Prior to this intervention, the animal needed to be anesthetized and given analgesic medication as described above. Then, the abdomen was re-opened and the intestines were carefully placed on a moist compress. One after another, the liver lobes had to be carefully separated and exposed so that one could clearly visualize the common hepatic artery that is dividing into the A. hepatica propria and the A.

gastroduodenalis, on the latter of which a ligature was set as far away from the branch as possible. Now, the common hepatic artery was clamped, to temporarily disrupt the blood flow to the liver. At this stage, the actual injection was carried out: carefully, the A. gastroduodenalis was punctured with a 30G needle under microscopic visual guidance. After administration of 500µl of therapeutic agent, a second suture was set on the A. gastroduodenalis, this time as close to the branch as possible such that the former puncture site was cut off from the circulation and post-interventional bleeding could be avoided.
(The now discontinued gastroduodenal artery is not needed for survival of the animal, as there are collaterals supplying the distal stomach and the duodenum.)
Finally, the clamp was removed from the common hepatic artery and, after making sure there was no remarkable bleeding, the intestines were re-localized into the abdomen, and sutures were set as described above. After this procedure, the animal was closely monitored and again released into veterinary care (Shinozaki, Ebert et al. 2004).

4.14 Statistical analysis:

Data analysis was carried out using GraphPad Prism software (GraphPad Software, CA, 205 USA)

5 Results

5.1 Titration of optimum Fe/pfu ratio

As a first step, the optimal ratio between infectious viral particles and magnetic nanoparticles (MNPs) was assessed by testing a wide range of iron to plaque forming unit (Fe/pfu) ratios (from 0 to 5000fg Fe/pfu) and examining complex size and charge. Afterwards the range between 0 and approximately 1000fg Fe/pfu was examined in detail by performing the magnetic sedimentation assay.

5.1.1 Size and charge measurements

Consistent with the fact that VSV is negatively charged at neutral pH (Espinoza, Schumann et al. 2004), and that PEI-Mag2 are known to have a strong positive charge of approximately +55mV (Mykhaylyk, Antequera et al. 2007), the charge measurements of VSV-MNP complexes revealed an increase in zeta potential coinciding with rising levels of PEI-Mag2-particles added. While VP alone (without addition of Fe) had a zeta potential of -10,97 mV (SD 0,34), as little as 19,5 fg Fe/pfu led to neutralization of the VSV-MNP complex, and from 156 fg Fe/pfu onward, a plateau at around +15mV was reached. At 312 fg Fe/pfu the zeta potential was 15,10 mV (SD 0,50). (Figure 7)

Examination of the particle sizes showed that VP alone had a hydrodynamic diameter of 162,93nm. With the addition of PEI-Mag2 particles, complexes formed and size increased to 1,5 µm with the addition of Fe particles in the range of 19,5 - 312 fg Fe/pfu. At even higher levels of PEI-Mag2 per infectious VP, the observed size of the complexes dropped to a mean diameter of 378,8 nm at a ratio of 5000 fg Fe/pfu (data not shown).

The number of PEI-Mag2-particles per complex, as calculated from the magnetic moment of the complex (see 4.6; figure 7, bottom) increased with its size. As can be seen, complexes that formed at a ratio between 19,5 and 312 fg Fe/pfu were relatively large and contained high amounts of PEI-Mag2 particles, consequently leading to a strong magnetic responsiveness.

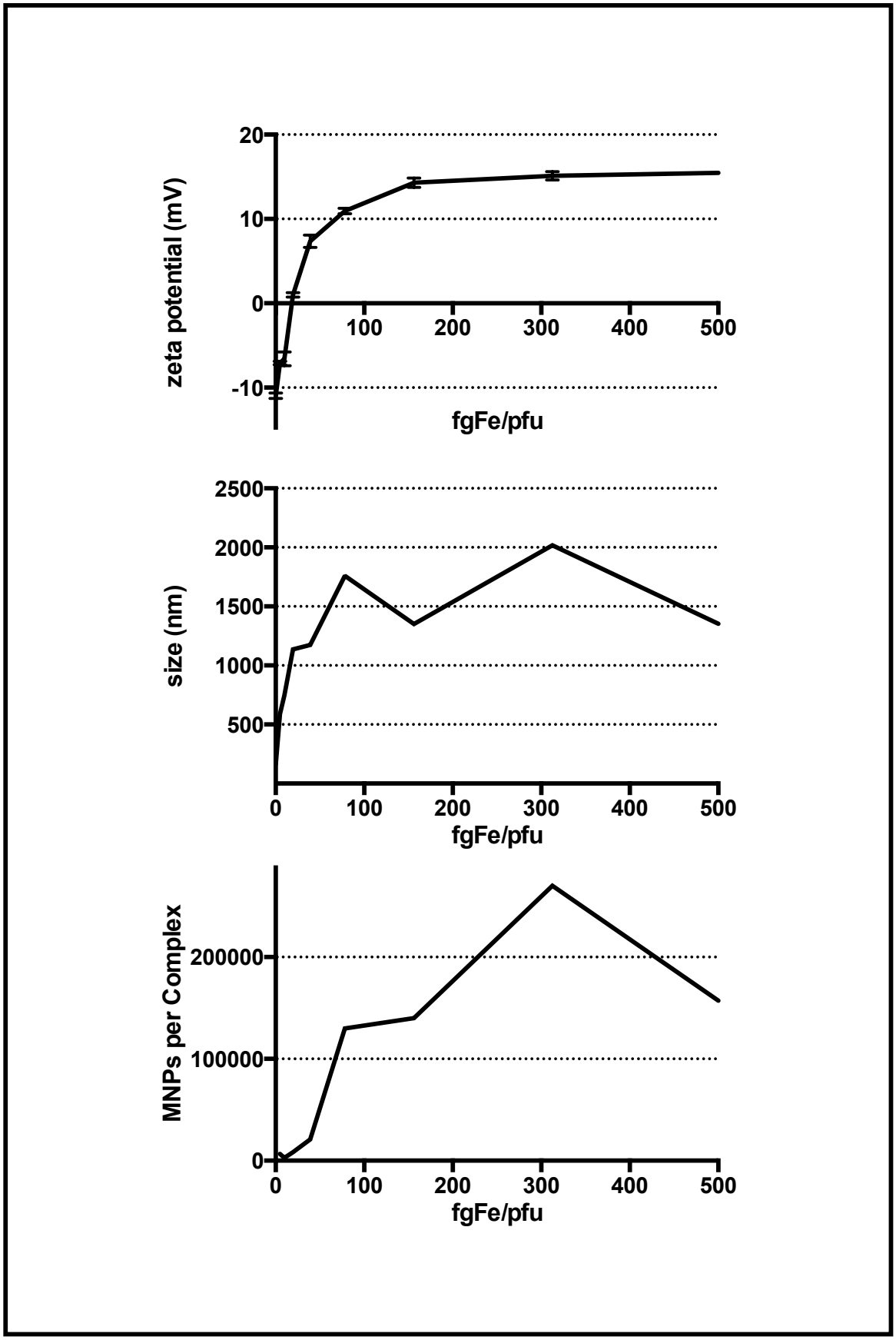

Figure 7: Size, charge and number of MNPs bound to the complex in relation to the iron/pfu-ratio in fgFe/pfu.

5.1.2 Virus binding

To quantify more precisely the VP binding capacity, complexes were formed at different ratios, followed by magnetic sedimentation. The binding capacity was estimated by quantifying the titer of unbound virus remaining in the supernatant and subtracting from the total amount of virus added.

As expected, the virus titer in the supernatant continuously decreased with the addition of MNPs from 10 to 312 fg Fe/pfu, demonstrating that increasing numbers of VSV particles became bound to the complexes and magnetically sedimented. Interestingly, when adding more MNPs per VP, the virus titer in supernatant increased again ($4{,}4 \times 10^5$ TCID50 at 1250 fg Fe/pfu versus $3{,}9 \times 10^{\wedge 4}$ TCID50 at 312 fg Fe/pfu.)

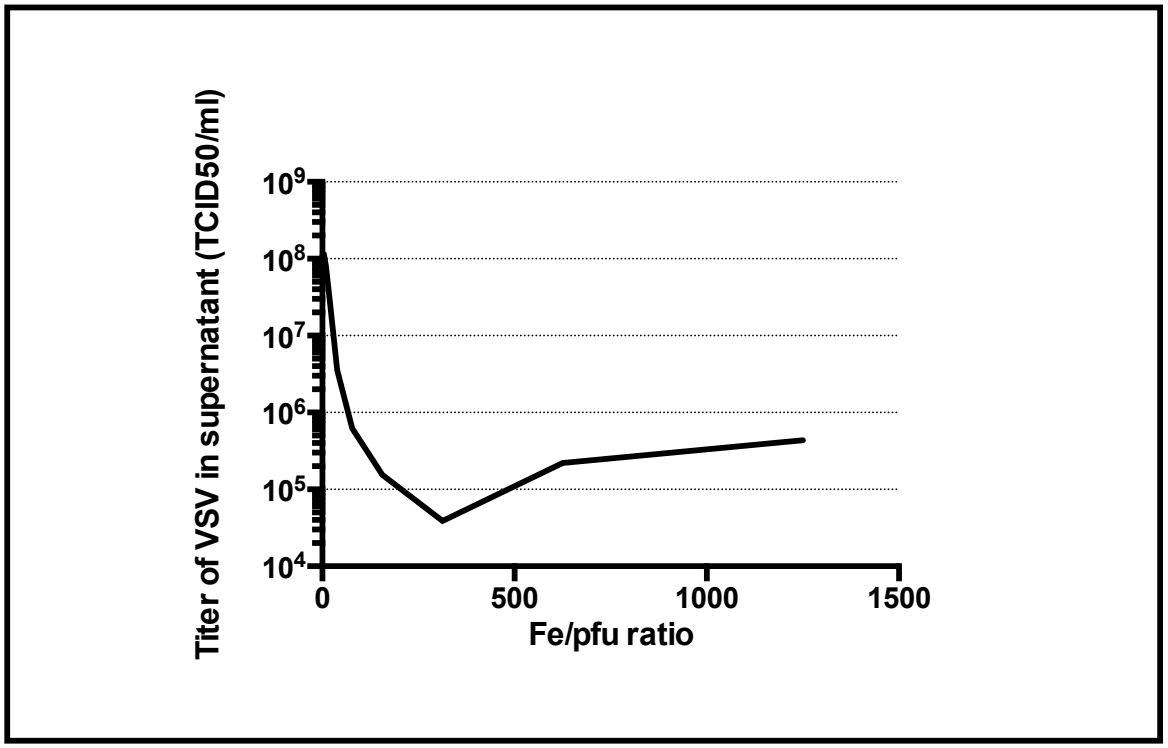

Figure 8: Amount of virus in the supernatant after magnetic sedimentation of VSV-PEIMag2 complexes, created at different Fe/pfu-ratios.

5.2 Negative staining electron microscopy

To analyze VSV-MNP complexes morphologically, a negative staining electron microscopy (NSEM) approach was chosen as the standard method for visualization (Gentile and Gerdelblom 2014). The resulting NSEM images of the VSV-PEI-Mag2-complexes, formed at a ratio of 300 fg Fe/pfu, revealed entire VP surrounded by PEI-Mag2 particles and assembled into large complexes of approximately 1,5 µm in longest diameter. This observation is consistent with the results from Zetasizer measurements.

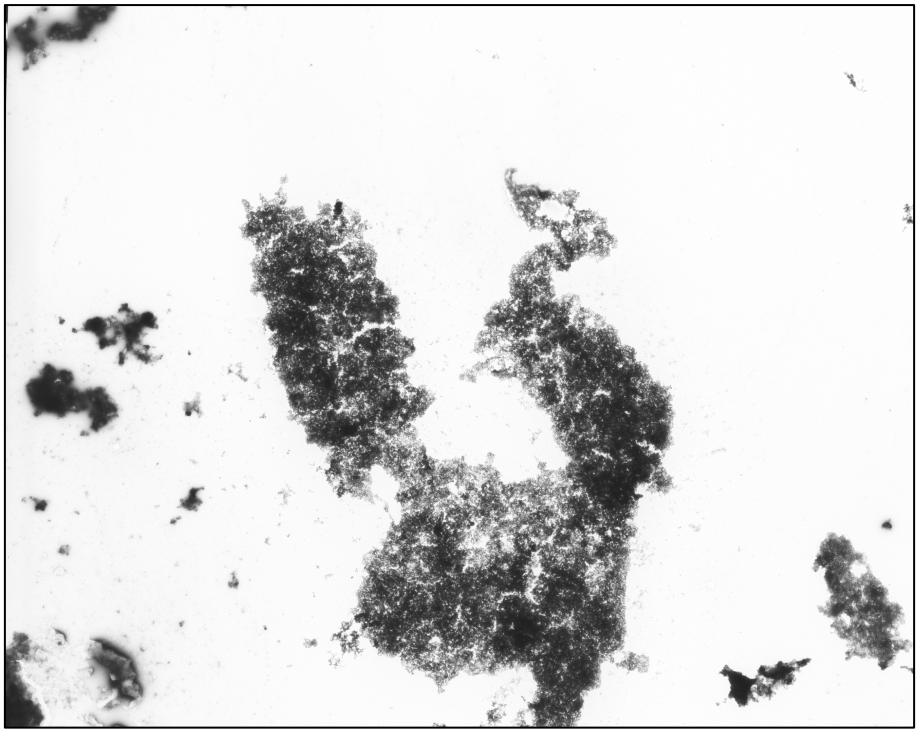

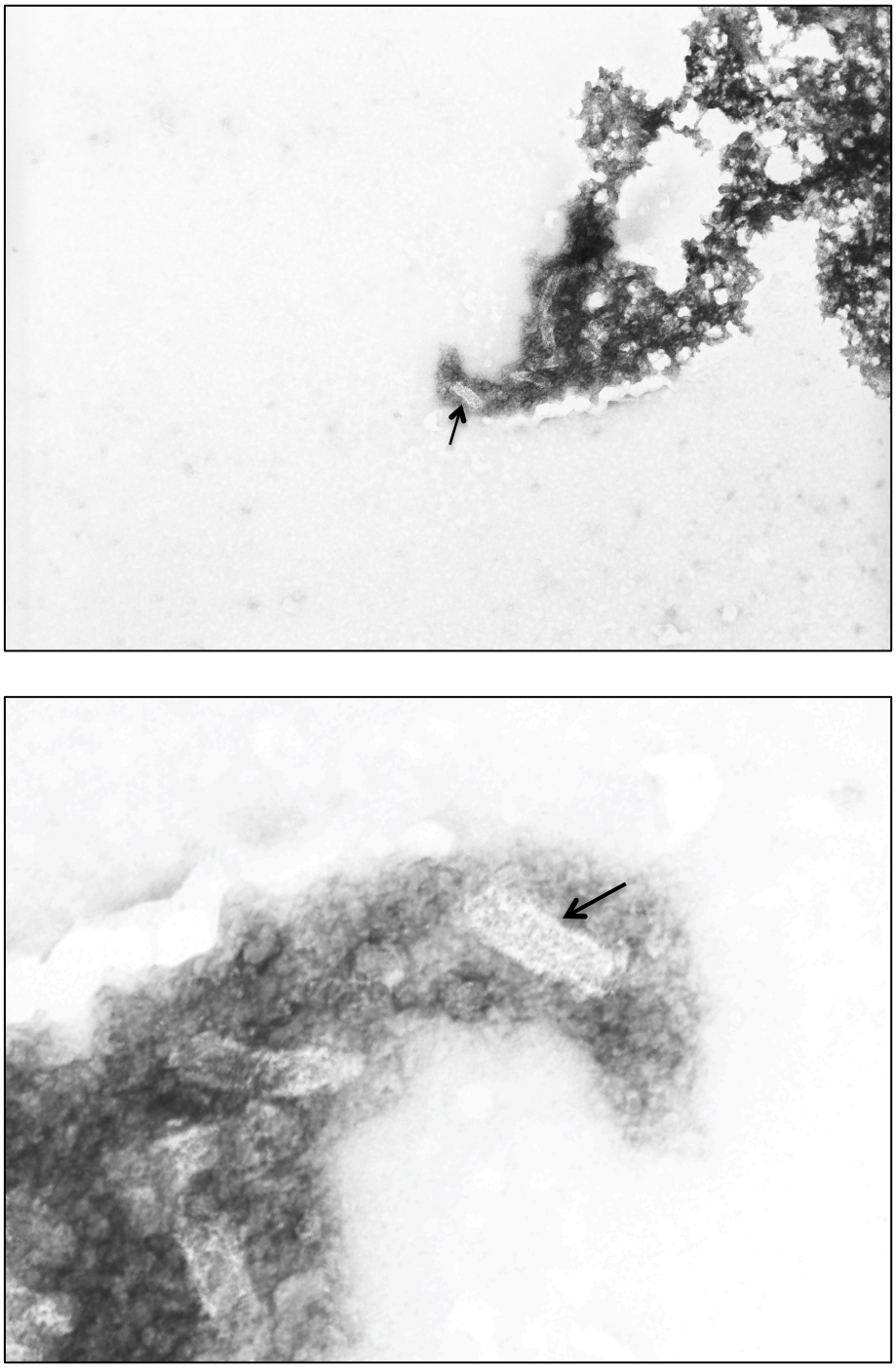

Figure 9: Negative staining electron microscopy of VSV-PEIMag2-Complexes formed at 300fgFe/pfu, the arrow is indicating a VSV particle. (3.150x/20.000x/50.000 x magnification); Pictures taken at Veterinarian Pathology Department, LMU, München.

5.3 Polymer testing

After establishing the optimal PEI-Mag2 to VSV particle ratio of 300 fg Fe/pfu (see Discussion) we next wanted to test the capacity of different shielding polymers to reverse surface charge and thus increase VSV-MNP stability and optimize pharmacokinetics, such as the in vivo circulation time.

5.3.1 Size and charge

In order to determine the size and charge of VSV-MNP complexes, a Zeta-Sizer was employed. Although some variation was noted for all employed polymers at lower ratios (see figure 10), in general, VSV-MNP complex size was not affected by shielding. At polymer-to-iron (w/w) ratios bigger than 1, all complexes appeared to be stable and did not aggregate to larger complexes.

Looking at the charge of the differently shielded complexes (see figure 11), the expected neutralization of the positive charge of the complexes by the anionic polymers could be observed. At a polymer-to-iron ratio of 10, all of the tested shielding complexes showed a negative charge, although P6YE5C was only able to reduce the charge to -7,26mV (SD 0,66), whereas the three other polymers showed a stronger effect with a net charge of more than -20mV each.

Of the polymers tested, hyaluronic acid was the most effective in neutralizing the charge of the complexes. With a polymer-to-iron (w/w) ratio of as low as 0,03, the charge of the HA-shielded complexes was at a negative value. PAGA and Poly-GAL achieved charge reversal of the complexes at ratios of around 0,20 each.

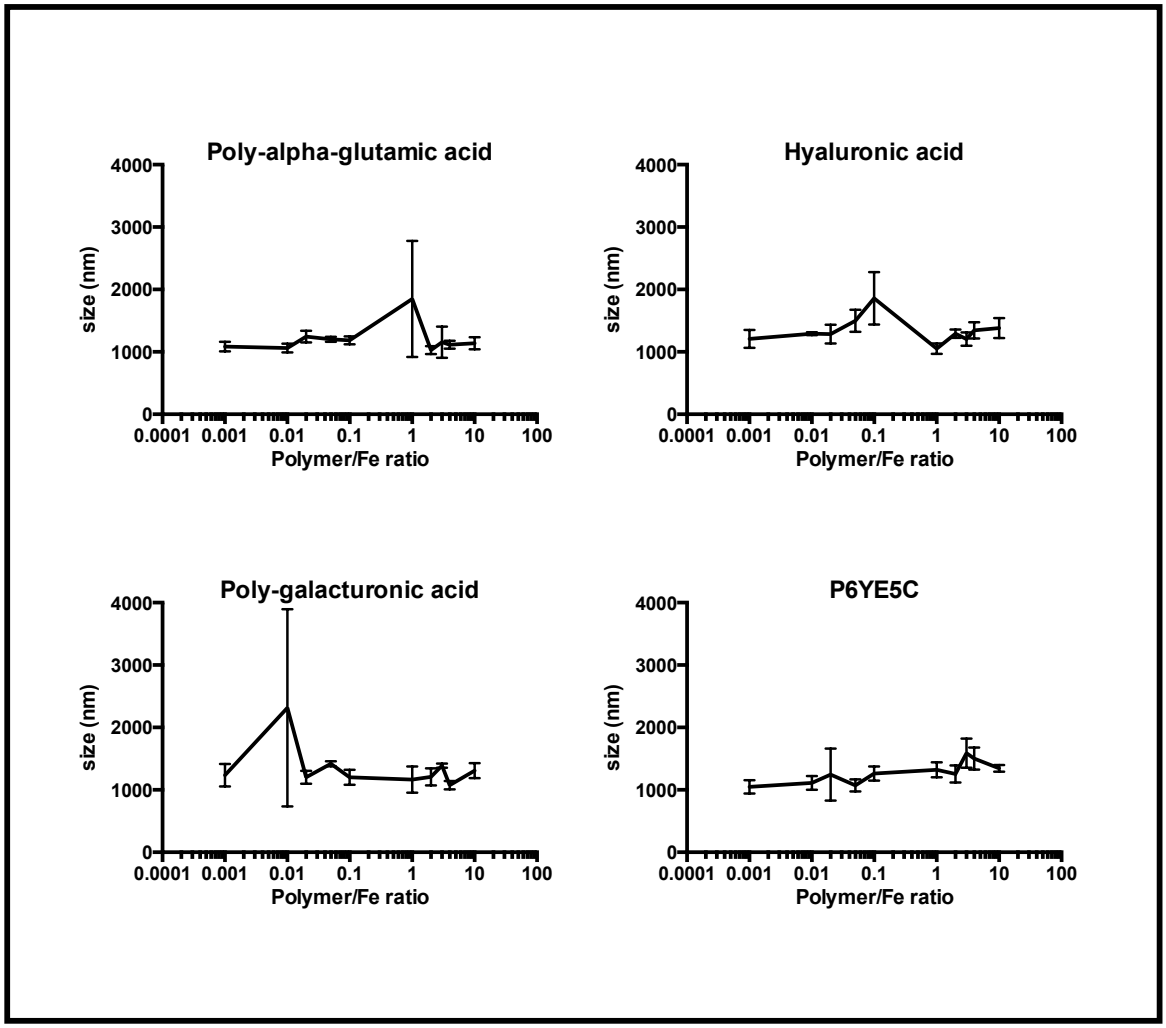

Figure 10: Shielding of VSV-PEIMag2 complexes with PAGA, HA, PolyGAL and P6YE5C at different shielding ratios; complex size.

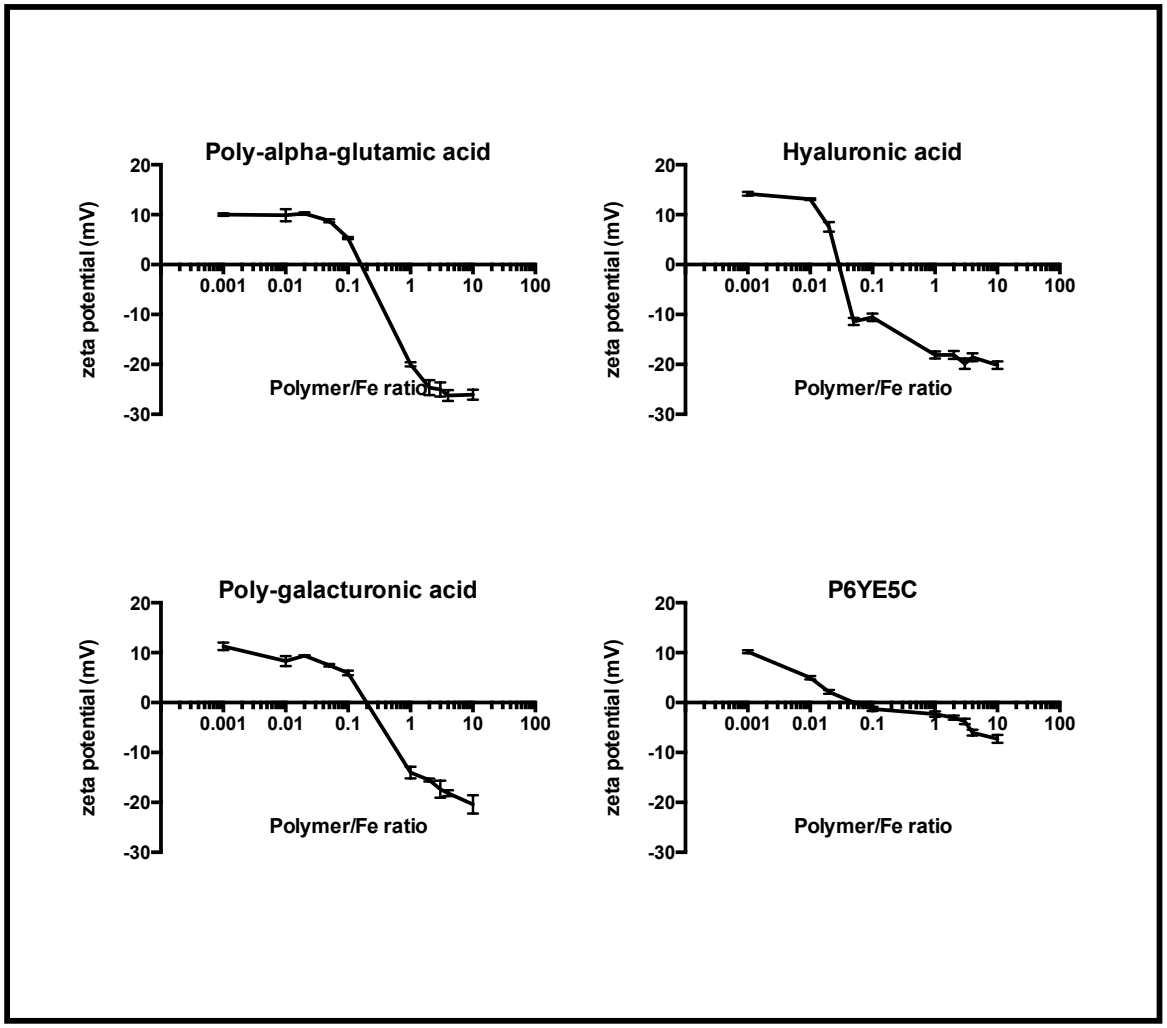

Figure 11: Shielding of VSV-PEIMag2 complexes with PAGA, HA, PolyGAL and P6YE5C at different shielding ratios; complex charge.

5.3.2 Infectivity in Morris hepatoma cells

After completing Zeta-Sizer measurements, the next step was to examine the complexes' ability to enter and replicate in cells after shielding. As can be seen in Figure 12, infection of HA-shielded complexes with and without a magnetic field led to a strong GFP signal, indicating an effective transduction of the GFP-encoding viral RNA in both cases. However, the signals were stronger upon magnetic field application, showing that the VSV-PEIMag2-HA complexes were magnetically attracted to the cells and thus able to infect with higher efficiency. The HA concentration range tested had no major effect on the infectivity and replication, though the charge of the complexes changed dramatically (see figure 11). Even without application of a magnetic field, a high concentration of shielding polymers did not prevent the complexes from entering the cells, which is in stark contrast to previous results with adenoviral complexes (unpublished data by O. Mykhaylyk). In contrast, in VSV-PEIMag2-PolyGAL complexes at high polymer-to-iron (w/w) ratios of 10:1 we observed the expected shielding effect in the absence of a magnetic field. Cells appeared healthy and showed no signs of VSV infection, as determined by light microscopy, see Figure 13.

With VSV-PEIMag2-P6YE5C complexes, there was no such inhibition to be observed, and VSV-PEIMag2-PAGA complexes showed only a slight inhibition (Figure 14 and 15).

All in all, HA showed the most promising performance: it did not inhibit the complexes from entering the cells, and it proved to be more effective in neutralizing and reversing the charge than the other examined anionic shielding polymers.

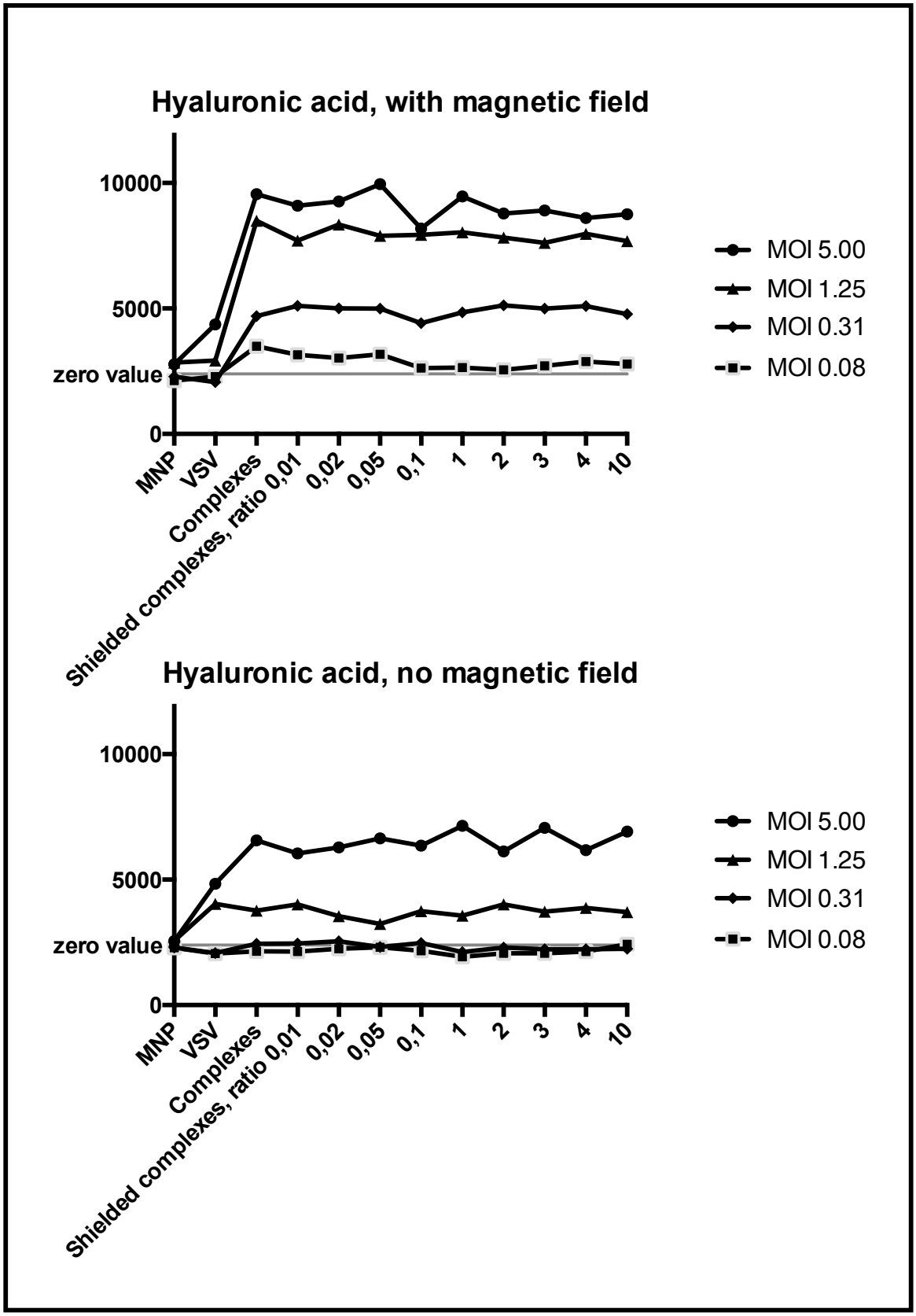

Figure 12: After infection with VSV-PEIMag2-HA-Complexes, McA-RH7777 cells produced a significant amount of GFP after 10 h of incubation. Also here, infection in the magnetic field as well as infection without application of a magnet both led to a strong GFP signal, indicating an effective transduction of the GFP-encoding viral RNA in both cases. However, the signal under application of the magnetic field is substantially higher, showing that the VSV-PEIMag2-HA-Complexes are magnetically attracted to the cells and thus are able to infect at a higher efficiency.

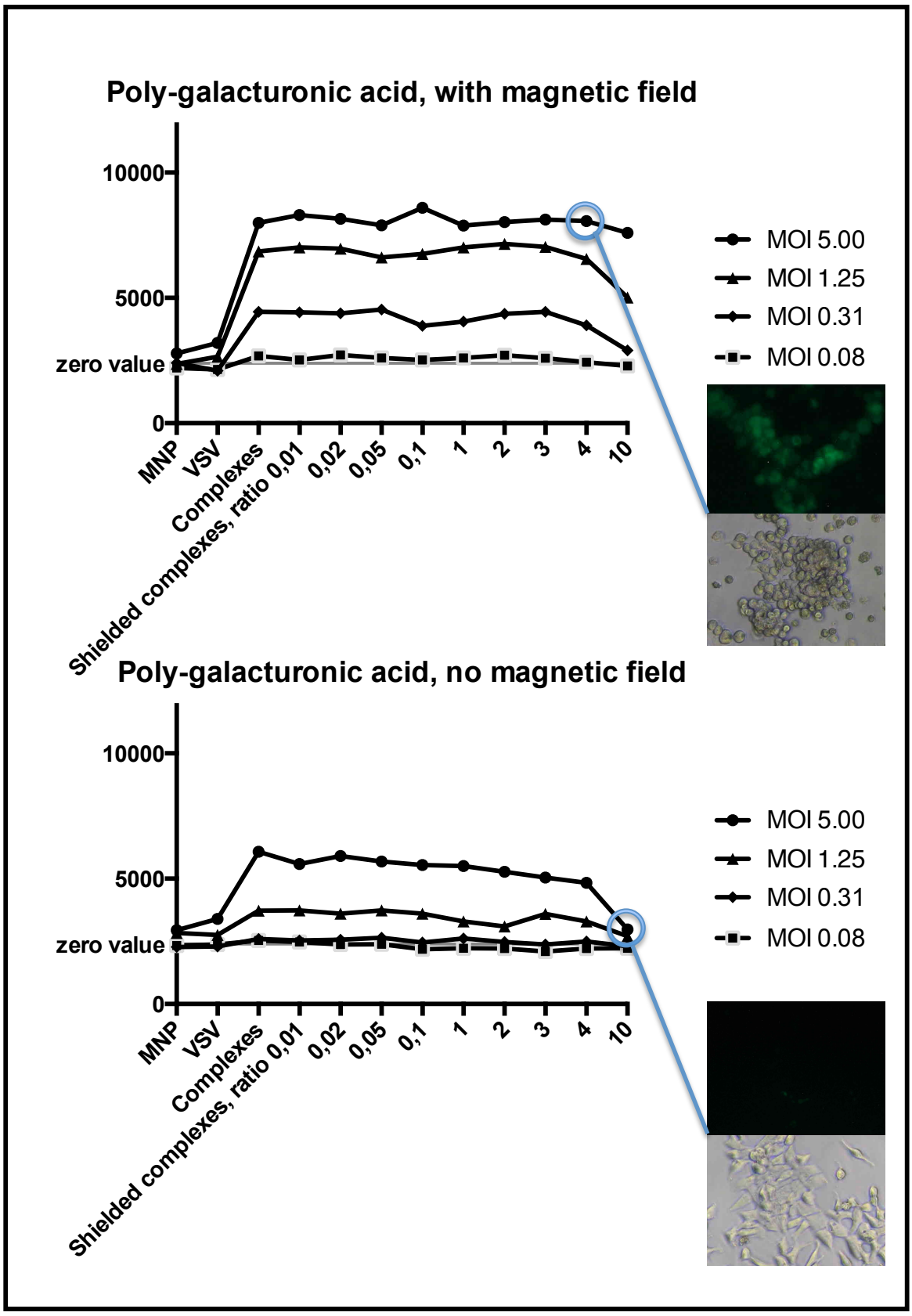

Figure 13: Signal intensity in fluorescent units, representing GFP expression in Morris Hepatoma cells for MNP, VSV, VSV-MNP-complexes and complexes shielded with Poly-Galacturonic acid in different ratios. The inserted images show fluorescence and light microscopy pictures of the respective samples indicated by the blue circle.

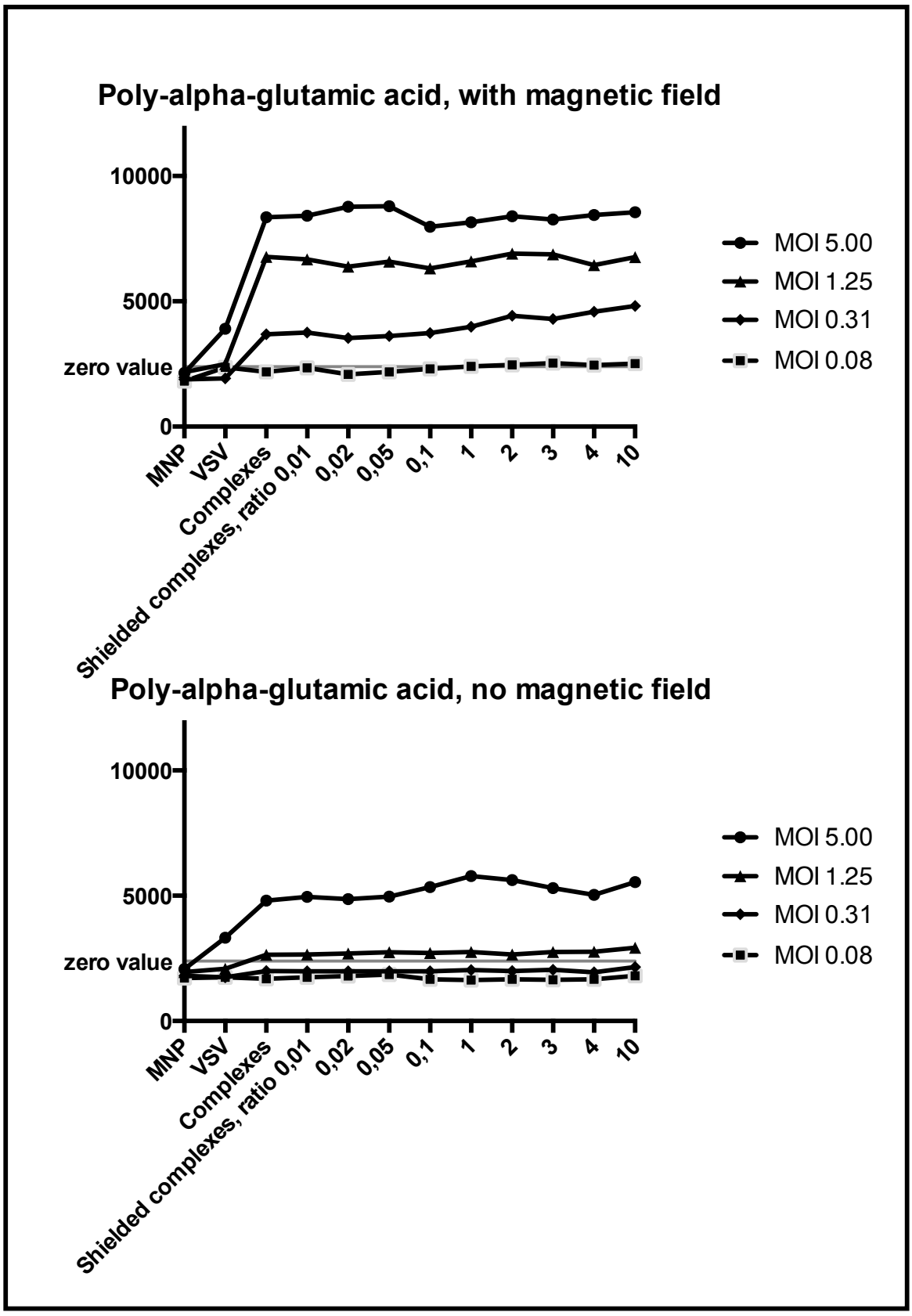

Figure 14: Signal intensity in fluorescent units, representing GFP expression in McA-RH7777 cells for MNP, VSV, VSV-MNP-complexes and complexes shielded with Poly-alpha glutamic acid in different ratios.

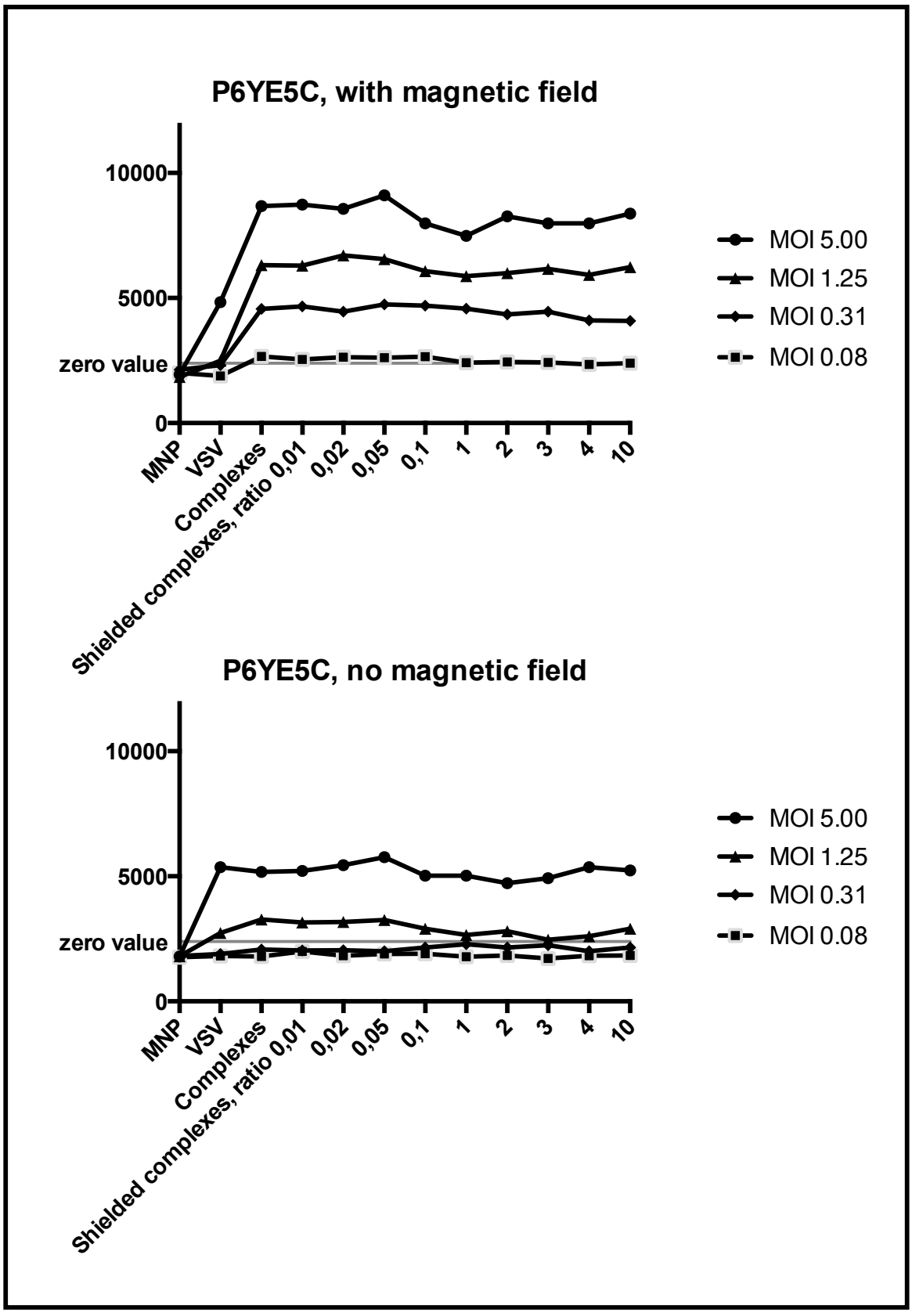

Figure 15: Signal intensity in fluorescent units, representing GFP expression in McA-RH7777 cells for MNP, VSV, VSV-MNP-complexes and complexes shielded with P6YE5C in different ratios.

5.3.3 Protection against neutralizing Antiserum

Next, to test the shielding effect of negatively charged polymers against inactivation by neutralizing antiserum, a neutralizing antibody assay was performed.

While VSV alone was highly susceptible to inactivation by the plasmatic immune system at an antiserum concentration of 0,04%, VSV-MNP complexes without shielding required a higher concentration of 0,14% (Figure 16). Highest concentrations were required for inactivation of VSV-PEIMag2-HA(0,1) and VSV-PEIMag2-HA(10). In detail 0,19% antiserum was required to neutralize the complexes with polymer-to-iron ratio of 0,1 and 0,16% for the fully shielded complexes at a ratio of 10. The p-value (paired t-test) for VSV vs. VSV-PEIMag2-HA(10) was p= 0,0372.

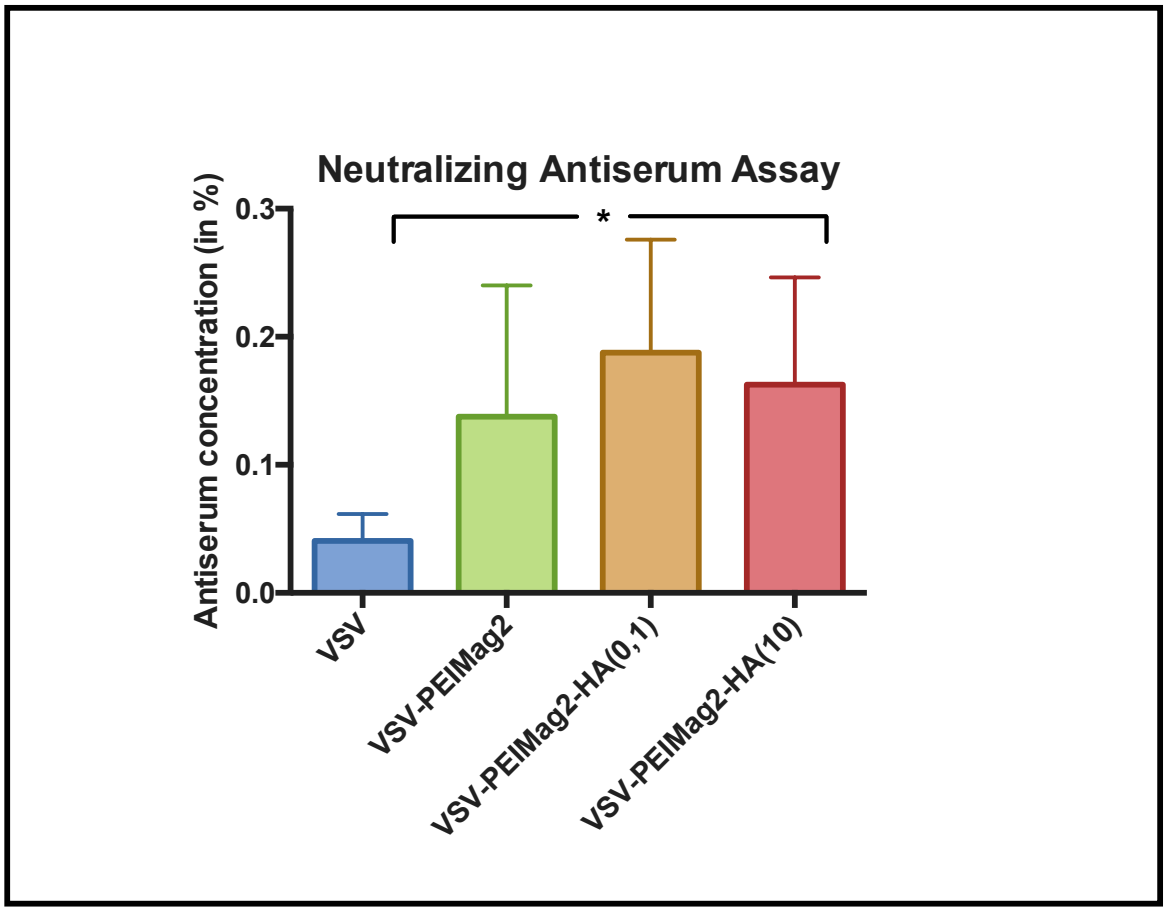

Figure 16: VSV, VSV-PEIMag2 and VSV-PEIMag2-HA (at low and high dose of Hyaluronic acid shielding) where incubated in Anti-VSV rat serum for 120 minutes, followed by a TCID50-based assay to examine the highest serum titer at which there was no CPE to be observed. Shielding with high amounts of hyaluronic acid ("VSV-PEIMag2-HA(10)") led to a significant increase in antiserum titer necessary to inactivate the virus. n=5; p=0.0372.

5.4 In-vivo application of the optimized VSV-MNP complex

5.4.1 Blood half life time

To test the in vivo shielding effect of HA, 10^7pfu of VSV, VSV-PEIMag2 or VSV-PEIMag2-HA(10) complexes were injected into the tail vein of buffalo rats. In the VSV group, the exponential decay fitting curve (dotted line) showed a relatively fast degradation of the viral particles, especially in the first minutes. With the complexed VPs (VSV-PEIMag2), this exponential decay followed a less steep curve and showed slower virus clearance when using iron-containing complexes. In the VSV-PEIMag2-HA(10) group, the initial degradation was the lowest. These results are shown in Figure 17. It should be highlighted that there was a broad inter-individual variation in VSV titers, resulting in large standard deviations. In the graph, the results range is plotted. Regardless, the tendency towards earlier removal from the blood for VSV alone can clearly be seen.

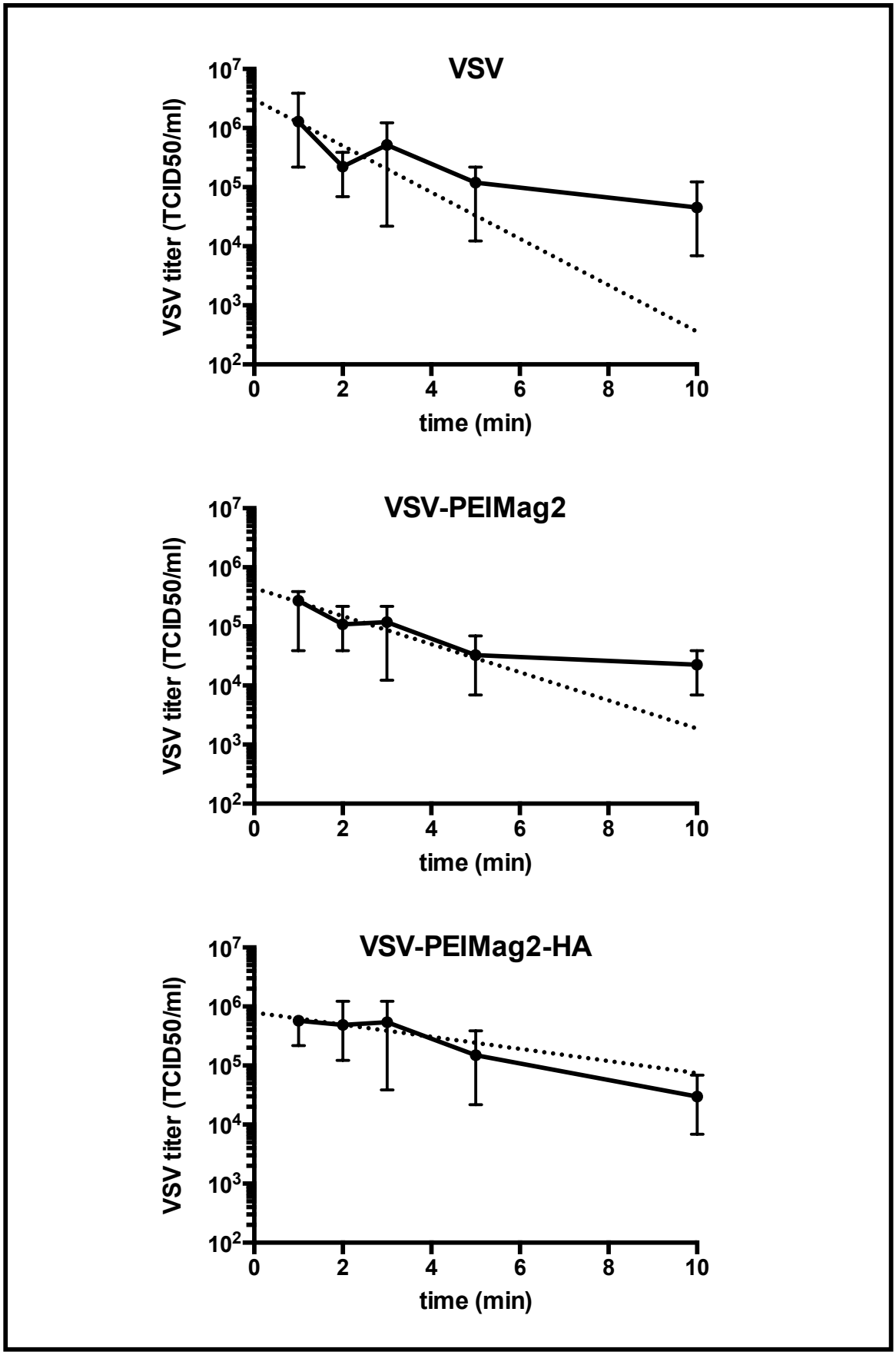

Figure 17: Full-blood VSV titer in Buffalo rats after injection of 10^7pfu of VSV, VSV-PEIMag2 or VSV-PEIMag2-HA, measured at 1,2,3,5 and 10 minutes after injection. The dotted lines show the exponential decay fitting curves. n=4 for the VSV and VSV-PEIMag2-HA and n=3 for the VSV-PEIMag2 group. The error bars show the results range.

5.4.2 First in vivo therapy experiments and outlook on future studies

In parallel to the described experiments, in vivo application of VSV-MNP complexes in tumor bearing rats was initiated, to test its feasibility. Figure 18 shows preliminary data from Almstätter et al (Almstatter, Mykhaylyk et al. 2015), where intratumoral injection of VSV-MNP-complexes led to clearly measureable iron-induced MRI signal loss in buffalo rats bearing orthotopic HCC lesions.

Future studies will aim at standardized application of the technique presented in this thesis and at evaluating the performance of VSV, VSV-PEIMag2 and and VSV-PEIMag2-HA(10) in a larger therapy and survival study.

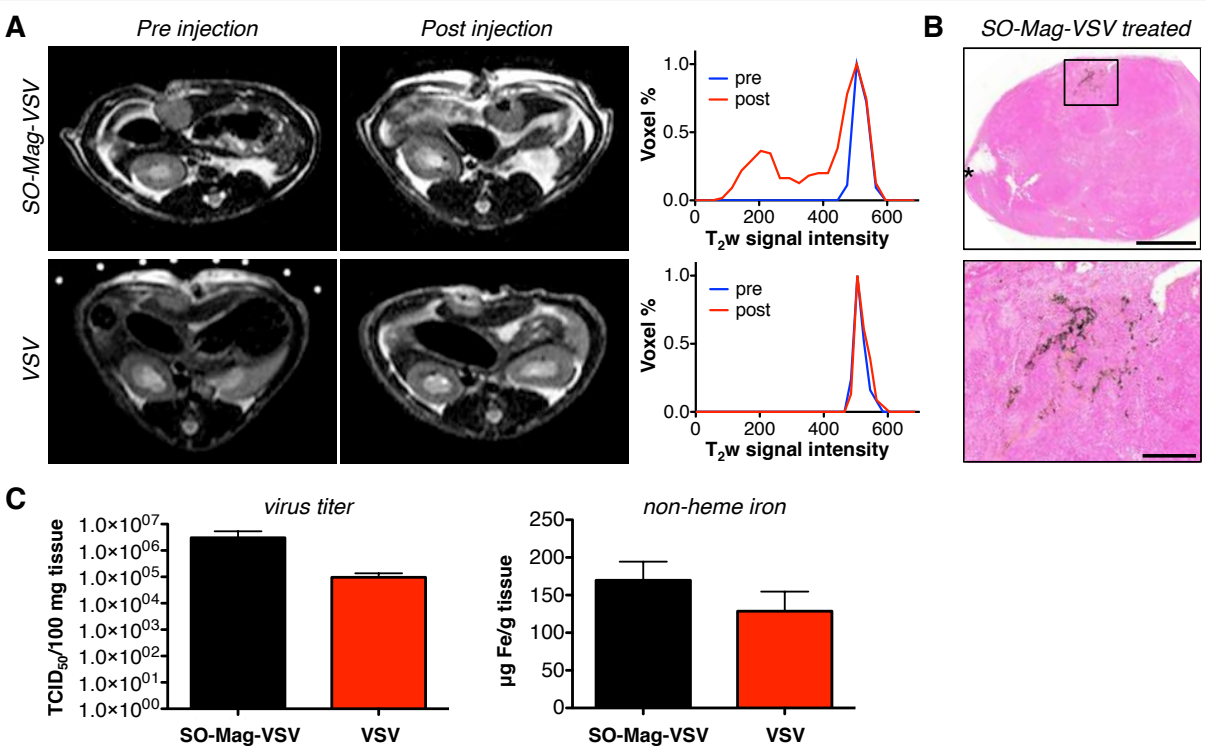

Figure 18: ***In vivo targeting of SO-Mag-VSV complexes. A*** *Pre- and post-injection T2-weighted images of orthotopic HCC after SO-Mag-VSV (top row) or free VSV (bottom row) injection. The corresponding histograms (A, right) illustrate the signal loss after magnetic complex application only.* ***B*** *Overview (top) and high magnification micrographs of prussian blue staining after SO-Mag-VSV injection. The asterisk marks the injection site and the magnet was placed above the boxed area (top); scale bars 2,000 µm (top) and 500 µm (bottom), respectively.* ***C*** *Intra-tumoral virus titer and non-heme iron of whole tumors sampled 30 min post infection with SO-Mag-VSV complexes (n=4) and free VSV (n=3). From (Almstatter, Mykhaylyk et al. 2015)*

6 Discussion

An oncolytically active and magnetically responsive therapeutic agent was designed and tested. It was examined whether shielding with an anionic biopolymer is able to improve the agents´ pharmacokinetics and reduce immunogenicity in vivo.

An optimal ratio of approximately 300 fg Fe/pfu for VSV-MNP complex formation was identified. Charge and size measurements revealed positive surface charge and stable complex formation with a strong magnetic moment at ratios between 78 and 625 fg Fe/pfu. The observed size of the complexes dropped to a mean diameter of 378,8 nm at a ratio of 5000 fg Fe/pfu, which might be explained by unbound MNPs that might have influenced the average size measured.
VP binding experiments at a ratio of 312 fg Fe/pfu exhibited an excellent performance with 99,9% of the originally added VP bound in complexes and magnetically sedimented after 20 minutes in an external magnetic field.

VSV-MNP complexes had an approximate size of 1,5 µm, which can be considered relatively large for injection into the blood stream. Usually nanoparticles used for medical purposes range between 1 and 100 nm, following the definition of “nanoscale” (Webster 2006). However, in a recent FDA statement on nanotechnology, also larger particles were included, e.g. if they are hierarchically assembled (Hamburg 2012). Considering the fact that the smallest capillaries measure about 5 µm in diameter, even complexes of around 2 µm in size should be able to pass, if no significant aggregation occurs. Histologic samples of the lung of

three rats that received tail vein injections of VSV-MNP complexes showed no signs of embolism (data not shown).

There are several reports stating that positively charged particles injected into the bloodstream are in danger of aggregating with plasma proteins, resulting in fast elimination from the blood stream (Brigger, Morizet et al. 2004, Chertok, David et al. 2010). Therefore, a charge reversal was attempted by modification with anionic biopolymers (HA, PolyGAL, PAGA and P6YE5C). Depending on the respective polymer, shielding efficiency varied substantially. The observed high standard deviation in size at lower polymer concentrations might be explained by incomplete charge reversal resulting in a mixed population of positively and negatively charged complexes that form bigger aggregates (Malvern_Instruments 2004).
Importantly, despite charge reversal, complexes did not lose their ability to infect cells. Infectivity was as high with the application of an external magnetic field as for unshielded complexes, suggesting that shielding was not detrimental to VSV-MNP complex stability.

In theory there are major advantages of shielding VSV particles, such as with an anionic polymer. Firstly, shielding from the immune system would result in a longer blood half-life of the injected complex, thus increasing direct antitumor effectiveness due to longer circulation time (Croyle, Callahan et al. 2004, Tesfay, Kirk et al. 2013). Secondly, it would be advantageous to hide VP from the immune system in order to prevent active immunization (O'Riordan, Lachapelle et al. 1999). After active immunization, repeated administration of VSV could result in fast elimination due to pre-existing antibodies (Eto, Yoshioka et al. 2010). In the present work, it was shown that VSV alone was susceptible to antibody inactivation. Retention of infectivity of

VSV in the presence of neutralizing antibodies was significantly improved by covering the surface of the virus with MNPs, independent of HA-shielding. More than 4-fold higher concentrations of antiserum were needed for neutralization when VPs were complexed with MNPs as compared to that required for naked virus. HA shielding did not further improve shielding from neutralizing antibody binding, suggesting a strong effect of MNPs alone.

The finding that even high concentrations of shielding-polymer did not prevent internalization into McA-RH7777-cells contradicts prior findings of Mykhaylyk (unpublished data) and Obermann et al (Obermann 2014), where HA shielding did prevent cell internalization of adenovirus-MNP complexes in different cell lines, such as HUVECs. One possible explanation would be an active transport into the Morris Hepatoma cells, such as by the HA-receptor (CD44), which is known to be expressed strongly in HCC lesions, especially in poorly differentiated tumors (Endo and Terada 2000). CD44 expression has not been evaluated on McA-RH7777 cells to our knowledge. Another reason might be a high metabolism and an active transmembrane transport (Sell and Leffert 2008) of McA-RH7777 cells. An unspecific internalization mechanism would explain why also shielding with the other polymers (PolyGAL, PAGA, P6YE5C) showed no or only very little of the above-mentioned shielding effect on McA-RH7777-cells. However, good internalization into McA-RH7777 cells, be it with or without application of a magnetic field, can be considered advantageous, as they are the desired target cells for application in the rat hepatoma model for therapy studies.

The role of the immune system in oncolytic virotherapy is still subject of controversy (Prestwich, Errington et al. 2009). A strong immune response may cause fast

clearance of viral complexes from the circulation. On the other hand the induced immune response itself is, to a great extent, responsible for prolonged tumor lysis (Altomonte and Ebert 2012). In the presented work it was attempted to achieve a longer circulation time of the applied complexes by shielding with anionic biopolymers, which could successfully be performed as shown by the anti-VSV antibody assay, as well as by the whole blood half-life time experiment. Still, it can be assumed that there is an immune response induced by the VSV-PEIMag2-HA complexes, since higher levels of anti-VSV antibodies were able to reach the VSV particles and to inactivate them. The optimum balance between protection from an antiviral immune response and induction of a strong antitumor immune response to enhance tumor lysis will have to be further examined by future studies.

Despite the fact that VSV-MNP clearance time from the blood stream was prolonged by the addition of Hyaluronic acid, titers at early time-points were higher for naked VSV (1,29E+06 TCID50/ml) compared to VSV-PEIMag2 (2,72E+05 TCID50/ml) and VSV-PEIMag2-HA complexes (5,72E+05 TCID50/ml). Although this finding was puzzling, one technical explanation for this observation could be that complexes containing multiple VPs behaved like one particle in the TCID50 assay.

A major concern with regard to future therapy studies is the placement of the external magnetic field gradient. Ideally, a magnetic field for magnetic targeting would direct any magnetically active particle in the body towards a desired target region, e.g. the tumor area. However, a force deriving from a magnetic field inhomogenity induced in a small magnetic particle can only be directed towards the inducing magnet and cannot “push away” the object (Heidsieck, Vosen et al. 2012). Thus it is physically impossible to form an external magnetic field that directs magnetic nanoparticles

from every part of the body towards a certain area at the same time. Several strategies have been proposed to address this challenge. One approach would be to use magnetic fields focused on larger vessel crossings to direct nanoparticles into either direction, as proposed by Riegler et al (Riegler, Wells et al. 2010, Riegler, Lau et al. 2011). Another possibility would be the use of an external magnetic field from a permanent magnet mounted outside the body as close to the tumor as possible, as shown by Chertok et al (Chertok, David et al. 2010). This would be practically the most simple, but only applicable for tumors close to the body surface. Conveniently, the Morris hepatoma model used in this study involves implanted HCC nodules that can be seeded directly under the liver capsule and are therefore amenable to this kind of magnetic targeting strategy. Theoretically, it also would be an option to implant a magnet directly in the tumor region as performed for example by Zhang et al (Zhang, Li et al. 2012), enabling the possibility to direct magnetically active agents in this area and allowing for repeated applications. However, this would be a very invasive technique.

There are drawbacks and limitations regarding the presented study that should be kept in mind. VSV-PEIMag2-HA complexes remain magnetically active and infective for at least 3h. However, VSV-PEIMag2-HA complex stability has not been tested at later time points, and others (Tresilwised, Pithayanukul et al. 2010) have shown MNP-Virus complex aggregating at later time points.
Shielding with HA did not further improve the beneficial effects of complexation with MNPs on antiserum inactivation. There was no significant effect of either MNP or MNP+HA-shielding on circulation time to be observed, and the tendency towards a prolongation of circulation time is low and only seen in the first minutes after

application. Therefore, the benefit of the additional shielding component to the complexes needs to be further investigated.

Another drawback could be the overall complexity of the intervention. The animal experiment presented in this study needs to be performed with microsurgical equipment and by experienced personnel. The critical time-point is the intra-arterial injection during application of the magnetic field, which can be technically challenging. However, theoretical future human application could be facilitated by the larger proportions and the application of the well-established technique of hepatic artery catheterization via the femoral artery (as performed during the TACE-procedure).

7 Conclusion

The results in this study show the possibility of complexation of VSV, magnetic nanoparticles and hyaluronic acid to form a therapeutic agent (VSV-PEIMag2-HA) that is oncolytically active and can be magnetically targeted. Additionally, the presented complexes demonstrate improved resistance to antibody inactivation and elimination from the blood stream. A theoretical application for therapy of human HCC and a specific concept for therapy studies using an HCC rat model were presented. Although technical and practical hurdles (i.e. complex stability, design of the external magnetic field) still need to be overcome, these preliminary results are promising and warrant further examination in future in-vivo therapy studies.

8 Sources

Alexiou, C., R. Jurgons, R. J. Schmid, C. Bergemann, J. Henke, W. Erhardt, E. Huenges and F. Parak (2003). "Magnetic drug targeting--biodistribution of the magnetic carrier and the chemotherapeutic agent mitoxantrone after locoregional cancer treatment." J Drug Target **11**(3): 139-149.

Almstatter, I., O. Mykhaylyk, M. Settles, J. Altomonte, M. Aichler, A. Walch, E. J. Rummeny, O. Ebert, C. Plank and R. Braren (2015). "Characterization of magnetic viral complexes for targeted delivery in oncology." Theranostics **5**(7): 667-685.

Altomonte, J., R. Braren, S. Schulz, S. Marozin, E. J. Rummeny, R. M. Schmid and O. Ebert (2008). "Synergistic antitumor effects of transarterial viroembolization for multifocal hepatocellular carcinoma in rats." Hepatology **48**(6): 1864-1873.

Altomonte, J. and O. Ebert (2012). "Replicating viral vectors for cancer therapy: strategies to synergize with host immune responses." Microb Biotechnol **5**(2): 251-259.

Anton, M., A. Wolf, O. Mykhaylyk, C. Koch, B. Gansbacher and C. Plank (2012). "Optimizing adenoviral transduction of endothelial cells under flow conditions." Pharm Res **29**(5): 1219-1231.

Balachandran, S. and G. N. Barber (2000). "Vesicular stomatitis virus (VSV) therapy of tumors." IUBMB Life **50**(2): 135-138.

Binder, M. (2013). "TCID-50 calculator." Retrieved 15.10.2013, 2013, from http://www.klinikum.uni-heidelberg.de/Downloads.126386.0.html.

Brigger, I., J. Morizet, L. Laudani, G. Aubert, M. Appel, V. Velasco, M. J. Terrier-Lacombe, D. Desmaele, J. d'Angelo, P. Couvreur and G. Vassal (2004). "Negative preclinical results with stealth nanospheres-encapsulated Doxorubicin in an orthotopic murine brain tumor model." J Control Release **100**(1): 29-40.

Britannica, E. (2015). "colloid." Retrieved 03 Februar, 2015, from http://www.britannica.com/EBchecked/topic/125898/colloid.

Burdick, J. A. and G. D. Prestwich (2011). "Hyaluronic acid hydrogels for biomedical applications." Adv Mater **23**(12): H41-56.

Chen, M. S., J. Q. Li, Y. Zheng, R. P. Guo, H. H. Liang, Y. Q. Zhang, X. J. Lin and W. Y. Lau (2006). "A prospective randomized trial comparing percutaneous local ablative therapy and partial hepatectomy for small hepatocellular carcinoma." Ann Surg **243**(3): 321-328.

Chertok, B., A. E. David and V. C. Yang (2010). "Polyethyleneimine-modified iron oxide nanoparticles for brain tumor drug delivery using magnetic targeting and intra-carotid administration." Biomaterials **31**(24): 6317-6324.

Chertok, B., B. A. Moffat, A. E. David, F. Yu, C. Bergemann, B. D. Ross and V. C. Yang (2008). "Iron oxide nanoparticles as a drug delivery vehicle for MRI monitored magnetic targeting of brain tumors." Biomaterials **29**(4): 487-496.

Choi, K. Y., G. Saravanakumar, J. H. Park and K. Park (2012). "Hyaluronic acid-based nanocarriers for intracellular targeting: interfacial interactions with proteins in cancer." Colloids Surf B Biointerfaces **99**: 82-94.

Croyle, M. A., S. M. Callahan, A. Auricchio, G. Schumer, K. D. Linse, J. M. Wilson, L. J. Brunner and G. P. Kobinger (2004). "PEGylation of a vesicular stomatitis virus G pseudotyped lentivirus vector prevents inactivation in serum." J Virol **78**(2): 912-921.

Decher, G. (1997). "Fuzzy Nanoassemblies: Toward Layered Polymeric Multicomposites." Science **277**(5330): 1232-1237.

Ebert, O., K. Shinozaki, T. G. Huang, M. J. Savontaus, A. Garcia-Sastre and S. L. Woo (2003). "Oncolytic vesicular stomatitis virus for treatment of orthotopic hepatocellular carcinoma in immune-competent rats." Cancer Res **63**(13): 3605-3611.

El-Serag, H. B. (2011). "Hepatocellular carcinoma." N Engl J Med **365**(12): 1118-1127.

El-Serag, H. B., J. A. Marrero, L. Rudolph and K. R. Reddy (2008). "Diagnosis and treatment of hepatocellular carcinoma." Gastroenterology **134**(6): 1752-1763.

Endo, K. and T. Terada (2000). "Protein expression of CD44 (standard and variant isoforms) in hepatocellular carcinoma: relationships with tumor grade, clinicopathologic parameters, p53 expression, and patient survival." J Hepatol **32**(1): 78-84.

Espinoza, L. A., K. R. Schumann, Y. Y. Luk, B. A. Israel and N. L. Abbott (2004). "Orientational behavior of thermotropic liquid crystals on surfaces presenting electrostatically bound vesicular stomatitis virus." Langmuir **20**(6): 2375-2385.

Eto, Y., Y. Yoshioka, T. Ishida, X. Yao, T. Morishige, S. Narimatsu, H. Mizuguchi, Y. Mukai, N. Okada, H. Kiwada and S. Nakagawa (2010). "Optimized PEGylated adenovirus vector reduces the anti-vector humoral immune response against adenovirus and induces a therapeutic effect against metastatic lung cancer." Biol Pharm Bull **33**(9): 1540-1544.

European Association For The Study Of The, L., R. European Organisation For and C. Treatment Of (2012). "EASL-EORTC clinical practice guidelines: management of hepatocellular carcinoma." J Hepatol **56**(4): 908-943.

Finsinger, D., J. S. Remy, P. Erbacher, C. Koch and C. Plank (2000). "Protective copolymers for nonviral gene vectors: synthesis, vector characterization and application in gene delivery." Gene Ther **7**(14): 1183-1192.

Fraser, J. R., T. C. Laurent and U. B. Laurent (1997). "Hyaluronan: its nature, distribution, functions and turnover." J Intern Med **242**(1): 27-33.

Gentile, M. and H. R. Gerdelblom (2014). "Electron microscopy in rapid viral diagnosis: an update." New Microbiol **37**(4): 403-422.

Gitto, S., G. Vitale, E. Villa and P. Andreone (2015). "Treatment of nonalcoholic steatohepatitis in adults: present and future." Gastroenterol Res Pract **2015**: 732870.

Grzeskowiak, B. F., Y. Sanchez-Antequera, E. Hammerschmid, M. Doblinger, D. Eberbeck, A. Wozniak, R. Slomski, C. Plank and O. Mykhaylyk (2015). "Nanomagnetic activation as a way to control the efficacy of nucleic acid delivery." Pharm Res **32**(1): 103-121.

Hajibagheri, A. N. (1999). Electron Microscopy: Methods and Protocols[Humana Press.

Hamburg, M. A. (2012). "Science and regulation. FDA's approach to regulation of products of nanotechnology." Science **336**(6079): 299-300.

Hastie, E. and V. Z. Grdzelishvili (2012). "Vesicular stomatitis virus as a flexible platform for oncolytic virotherapy against cancer." J Gen Virol **93**(Pt 12): 2529-2545.

Heidsieck, A., S. Vosen, K. Zimmermann, D. Wenzel and B. Gleich (2012). "Analysis of Trajectories for Targeting of Magnetic Nanoparticles in Blood Vessels." Mol Pharm.

Howlader N, N. A., Krapcho M, Neyman N, Aminou R, Altekruse SF, Kosary CL, Ruhl J, Tatalovich Z, Cho H, Mariotto A, Eisner MP, Lewis DR, Chen HS, Feuer EJ, Cronin KA. (2012). "SEER Cancer Statistics Review, 1975-2009 (Vintage 2009 Populations)." from http://seer.cancer.gov/csr/1975_2009_pops09/.

Jan, K. M. and S. Chien (1973). "Role of surface electric charge in red blood cell interactions." J Gen Physiol **61**(5): 638-654.

Johnson, J. E., F. Nasar, J. W. Coleman, R. E. Price, A. Javadian, K. Draper, M. Lee, P. A. Reilly, D. K. Clarke, R. M. Hendry and S. A. Udem (2007). "Neurovirulence properties of recombinant vesicular stomatitis virus vectors in non-human primates." Virology **360**(1): 36-49.

Josefsson, A., H. Adamo, P. Hammarsten, T. Granfors, P. Stattin, L. Egevad, A. E. Laurent, P. Wikstrom and A. Bergh (2011). "Prostate cancer increases hyaluronan in surrounding nonmalignant stroma, and this response is associated with tumor growth and an unfavorable outcome." Am J Pathol **179**(4): 1961-1968.

Kim, J. E., J. Y. Shin and M. H. Cho (2012). "Magnetic nanoparticles: an update of application for drug delivery and possible toxic effects." Arch Toxicol **86**(5): 685-700.

Lichty, B. D., A. T. Power, D. F. Stojdl and J. C. Bell (2004). "Vesicular stomatitis virus: re-inventing the bullet." Trends Mol Med **10**(5): 210-216.

Lim, K. C., P. K. Chow, J. C. Allen, F. J. Siddiqui, E. S. Chan and S. B. Tan (2012). "Systematic review of outcomes of liver resection for early hepatocellular carcinoma within the Milan criteria." Br J Surg **99**(12): 1622-1629.

Llovet, J. M., S. Ricci, V. Mazzaferro, P. Hilgard, E. Gane, J. F. Blanc, A. C. de Oliveira, A. Santoro, J. L. Raoul, A. Forner, M. Schwartz, C. Porta, S. Zeuzem, L. Bolondi, T. F. Greten, P. R. Galle, J. F. Seitz, I. Borbath, D. Haussinger, T. Giannaris, M. Shan, M. Moscovici, D. Voliotis, J. Bruix and S. I. S. Group (2008). "Sorafenib in advanced hepatocellular carcinoma." N Engl J Med **359**(4): 378-390.

Lvov, Y., H. Haas, G. Decher, H. Mohwald, A. Mikhailov, B. Mtchedlishvily, E. Morgunova and B. Vainshtein (1994). "Successive Deposition of Alternate Layers of Polyelectrolytes and a Charged Virus." Langmuir **10**(11): 4232-4236.

Malvern_Instruments (2004). Zetasizer Nano Series User Manual. Worcestershire. WR14 1XZ United Kingdom, Malvern Instruments Ltd.

Mazzaferro, V., E. Regalia, R. Doci, S. Andreola, A. Pulvirenti, F. Bozzetti, F. Montalto, M. Ammatuna, A. Morabito and L. Gennari (1996). "Liver transplantation for the treatment of small hepatocellular carcinomas in patients with cirrhosis." N Engl J Med **334**(11): 693-699.

Melancon, M. P. and C. Li (2011). "Multifunctional synthetic poly(L-glutamic acid)-based cancer therapeutic and imaging agents." Mol Imaging **10**(1): 28-42.

Monsour Jr, H. P., E. Asham, R. S. McFadden, D. W. Victor III, B. Muthuswamy and I. Zaheer (2013). "Hepatocellular carcinoma: the rising tide from east to west—a review of epidemiology, screening and tumor markers." Translational Cancer Research **2**(6): 492-506.

Mykhaylyk, O., Y. S. Antequera, D. Vlaskou and C. Plank (2007). "Generation of magnetic nonviral gene transfer agents and magnetofection in vitro." Nat Protoc **2**(10): 2391-2411.

Mykhaylyk, O., T. Sobisch, I. Almstatter, Y. Sanchez-Antequera, S. Brandt, M. Anton, M. Doblinger, D. Eberbeck, M. Settles, R. Braren, D. Lerche and C. Plank (2012). "Silica-iron oxide magnetic nanoparticles modified for gene delivery: a search for optimum and quantitative criteria." Pharm Res **29**(5): 1344-1365.

Mykhaylyk, O., O. Zelphati, J. Rosenecker and C. Plank (2008). "siRNA delivery by magnetofection." Curr Opin Mol Ther **10**(5): 493-505.

Naik, S., R. Nace, G. N. Barber and S. J. Russell (2012). "Potent systemic therapy of multiple myeloma utilizing oncolytic vesicular stomatitis virus coding for interferon-beta." Cancer Gene Ther **19**(7): 443-450.

O'Riordan, C. R., A. Lachapelle, C. Delgado, V. Parkes, S. C. Wadsworth, A. E. Smith and G. E. Francis (1999). "PEGylation of adenovirus with retention of infectivity and protection from neutralizing antibody in vitro and in vivo." Hum Gene Ther **10**(8): 1349-1358.

Obermann, J. (2014). "Umhüllung magnetischer viraler Komplexe
Optimierung der viralen Transduktion von Endothel- und Muskelzellen unter statischen und Fließbedingungen."

Plank, C., O. Zelphati and O. Mykhaylyk (2011). "Magnetically enhanced nucleic acid delivery. Ten years of magnetofection-progress and prospects." Adv Drug Deliv Rev **63**(14-15): 1300-1331.

Polyak, B. and G. Friedman (2009). "Magnetic targeting for site-specific drug delivery: applications and clinical potential." Expert Opin Drug Deliv **6**(1): 53-70.

Prestwich, R. J., F. Errington, R. M. Diaz, H. S. Pandha, K. J. Harrington, A. A. Melcher and R. G. Vile (2009). "The case of oncolytic viruses versus the immune system: waiting on the judgment of Solomon." Hum Gene Ther **20**(10): 1119-1132.

Riegler, J., K. D. Lau, A. Garcia-Prieto, A. N. Price, T. Richards, Q. A. Pankhurst and M. F. Lythgoe (2011). "Magnetic cell delivery for peripheral arterial disease: A theoretical framework." Med Phys **38**(7): 3932-3943.

Riegler, J., J. A. Wells, P. G. Kyrtatos, A. N. Price, Q. A. Pankhurst and M. F. Lythgoe (2010). "Targeted magnetic delivery and tracking of cells using a magnetic resonance imaging system." Biomaterials **31**(20): 5366-5371.

Russell, S. J., K. W. Peng and J. C. Bell (2012). "Oncolytic virotherapy." Nat Biotechnol **30**(7): 658-670.

Sell, S. and H. L. Leffert (2008). "Liver cancer stem cells." J Clin Oncol **26**(17): 2800-2805.

Shinozaki, K., O. Ebert, C. Kournioti, Y. S. Tai and S. L. Woo (2004). "Oncolysis of multifocal hepatocellular carcinoma in the rat liver by hepatic artery infusion of vesicular stomatitis virus." Mol Ther **9**(3): 368-376.

Soheyla H, F. Z. (2013). "Effect of Zeta Potential on the Properties of Nano-Drug Delivery Systems - A Review." Trop J Pharm Res **April 2013; Volume 12** (Number 2): 255-273.

Tesfay, M. Z., A. C. Kirk, E. M. Hadac, G. E. Griesmann, M. J. Federspiel, G. N. Barber, S. M. Henry, K. W. Peng and S. J. Russell (2013). "PEGylation of vesicular stomatitis virus (VSV) extends virus persistence in blood circulation of passively immunized mice." J Virol.

Thrivikraman, K. V., R. L. Huot and P. M. Plotsky (2002). "Jugular vein catheterization for repeated blood sampling in the unrestrained conscious rat." Brain Res Brain Res Protoc **10**(2): 84-94.

Tresilwised, N., P. Pithayanukul, P. S. Holm, U. Schillinger, C. Plank and O. Mykhaylyk (2012). "Effects of nanoparticle coatings on the activity of oncolytic adenovirus-magnetic nanoparticle complexes." Biomaterials **33**(1): 256-269.

Tresilwised, N., P. Pithayanukul, O. Mykhaylyk, P. S. Holm, R. Holzmuller, M. Anton, S. Thalhammer, D. Adiguzel, M. Doblinger and C. Plank (2010). "Boosting oncolytic adenovirus potency with magnetic nanoparticles and magnetic force." Mol Pharm **7**(4): 1069-1089.

Unger, F., M. Wittmar and T. Kissel (2007). "Branched polyesters based on poly[vinyl-3-(dialkylamino)alkylcarbamate-co-vinyl acetate-co-vinyl alcohol]-graft-poly(d,l-lactide-co-glycolide): effects of polymer structure on cytotoxicity." Biomaterials **28**(9): 1610-1619.

Voeikov, V. L., E. V. Buravleva and S. E. Kondakov (2011). "Blood as an active colloidal system: The nonlinear nature of erythrocyte sedimentation in whole blood revealed by video recording with high spatial-temporal resolution." Moscow University Chemistry Bulletin **66**(4): 259-264.

Waly Raphael, S., Z. Yangde and C. Yuxiang (2012). "Hepatocellular carcinoma: focus on different aspects of management." ISRN Oncol **2012**: 421673.

Webster, T. J. (2006). "Nanomedicine: what's in a definition?" Int J Nanomedicine **1**(2): 115-116.

Zhang, Y., W. Li, L. Ou, W. Wang, E. Delyagina, C. Lux, H. Sorg, K. Riehemann, G. Steinhoff and N. Ma (2012). "Targeted delivery of human VEGF gene via complexes of magnetic nanoparticle-adenoviral vectors enhanced cardiac regeneration." PLoS One **7**(7): e39490.

9 Note of thanks/Danksagung

Abschließend möchte ich gerne all denjenigen danken, die an der Fertigstellung dieser herausfordernden, spannenden und bereichernden Arbeit beteiligt waren.

Besonderer Dank gebührt Univ.-Prof. Dr. Ernst J. Rummeny, Leiter des Instituts für diagnostische und interventionelle Radiologie, für die Ermöglichung der Promotion.

Außerdem möchte ich PD Dr. Rickmer Braren für die Überlassung des Themas, die optimale Betreuung über den gesamten Zeitraum, die Durchsicht des Manuskripts und die gute Zusammenarbeit danken.

Des Weiteren danke ich Dr. Jennifer Altomonte für das sorgsame Korrekturlesen und die vielen konstruktiven Ratschläge.

Allen Mitgliederen der AGs Braren, Ebert und Plank danke ich für die gute wissenschaftliche und zugleich kollegiale Arbeitsatmosphäre, insbesondere Dr. Olga Mykhaylyk, PD Dr. Oliver Ebert, Dr. Claudia Groß, Dr. Irina Heid, Dr. Katja Steiger, Isabella Almstätter, Juliane Dworniczak, Kim Bentrup, Iryna Skuratovska und Christoph Wörner.